Research Article

Citrullination at the Nuclear Localization Signal of the Inhibitor of Growth 4 (ING4) Interferes With its Binding to Importin α3

María Gabriela Álvarez-Rodríguez [1,†], Sonia Vega [2], Felipe Hornos [1], Augusto Fienco-Bacusoy [3], Olga Abian [2,4,5,6], Adrian Velazquez-Campoy [2,4,5,6,], Bruno Rizzuti [2,7,***], and José L. Neira [1,2,*,†]**

*1 - **IDIBE,** Universidad Miguel Hernández, 03202 Elche, Alicante, Spain*
*2 - **Instituto de Biocomputación y Física de Sistemas Complejos (BIFI),** Universidad de Zaragoza 50018 Zaragoza, Spain*
*3 - **Department of Physics,** University of Calabria, 87036 Rende, Italy*
*4 - **Instituto de Investigación Sanitaria Aragón (IIS Aragón),** Zaragoza, Spain*
*5 - **Centro de Investigación Biomédica en Red en el Área Temática de Enfermedades Hepáticas y Digestivas (CIBEREHD),** 28029 Madrid, Spain*
*6 - **Departamento de Bioquímica y Biología Molecular y Celular,** Universidad de Zaragoza 50009 Zaragoza, Spain*
*7 - **CNR-NANOTEC,** SS Rende (CS), Department of Physics, University of Calabria, 87036 Rende, Italy*

Correspondence to José L. Neira: *IDIBE, Edificio Torregaitán, Universidad Miguel Hernández, Avda. del Ferrocarril s/n, 03202 Elche, Alicante, Spain. adrianvc@unizar.es (A. Velazquez-Campoy), bruno.rizzuti@cnr.it (B. Rizzuti), jlneira@umh.es (J.L. Neira)*
https://doi.org/10.1016/j.jmb.2026.169877
Edited by Shixian Lin

Abstract

The inhibitor of growth 4 (ING4) acts as a tumor suppressor regulating chromatin structure. Due to this nuclear function, ING4 has a nuclear localization signal (NLS), which is recognized by the cellular translocation machinery mainly formed by proteins named importins, which include the isoform importin α3 (Impα3) to allow movement through the nuclear membrane. Peptidyl arginine iminohydrolases (PADIs) are enzymes involved in the posttranslational modification of arginine to citrulline. PADI4, one of the five isoforms of PADI in humans, citrullinates ING4 at the NLS region. We studied *in vitro* and *in silico* how the different degrees of citrullination affected binding of the NLS of ING4 to PADI4, Impα3 and its truncated species (ΔImpα3), lacking the importin binding domain, by using several biophysical techniques and molecular simulations. To that end, we synthesized eight peptides encompassing the NLS of ING4 (residues 130–152), with single, double and triple citrulline replacements at Arg132, Arg142 and Arg144. The peptides were monomeric and disordered, as tested by DOSY, 1D- and 2D-^{1}H NMR experiments. All the peptides were capable of binding to PADI4 with low micromolar affinities, but their affinity decreased as the fraction of citrullination increased. Moreover, all peptides could bind to both importin species with affinities in the low micromolar range, and their affinities were also dependent on the citrullination degree. The peptides targeted the canonical NLS binding site for cargo proteins of both importin species. These findings suggest that: (i) citrullination at the NLS

**Instituto de Biocomputación y Física de Sistemas Complejos (BIFI), Universidad de Zaragoza, 50018 Zaragoza, Spain
***CNR-NANOTEC, SS Rende (CS), Department of Physics, University of Calabria, 87036 Rende, Italy

might interfere with ING4 nuclear translocation; and (ii) successive citrullination at the NLS affected binding to PADI4.

Introduction

Citrullination is a post-translational modification (PTM) occurring in the presence of Ca^{2+} and catalyzed by L-arginine iminohydrolases (PADIs), a family of proteins also known as peptidylarginine deiminases (EC 3.5.3.15). PADIs intervene in apoptosis, tissue aging, nerve growth, inflammation, embryonic development, epithelial differentiation and transcriptional regulation of gene expression [1–6]. Furthermore, several immune diseases and many types of cancers are associated with an increased presence of some PADI isoforms and their citrullinated targets in different tissues [6–10]. PADI4 (Q9UM07) is one of the five isoforms found in humans. Among other cell locations, PADI4 is usually found in the cytoplasmic granules of eosinophils, neutrophils or macrophages, and in tumor cells, where PADI4 is highly expressed, either in the cytosol or in the nucleus, as we have previously shown for several types of cancer [11]. PADI4 is also involved in gene transcription and immune system modulation [6,12–15]. PADI4 modulates *p53* gene expression, as well as the expression of other *p53*-target genes [16,17]. We have recently reported that PADI4 binds to other key proteins involved in nuclear translocation and cancer development, such as importin α3 (Impα3) [18]; plakophilin 1 (PKP1) [19]; murine double minute 2 (MDM2) and some of its fragments [20,21]; the RING and YY1-binding protein (RYBP) [22]; and the Really Interesting New Gene protein 1B (RING1B), in particular with its C-terminal region (C-RING1B, residues 228–336 of the intact protein) [23]. We have also shown that PADI4 has an interactome that extends beyond proteins, being capable of binding also to lipids [24].

The human inhibitor of growth 4 (ING4) (Q9UNL4) belongs to the ING family of tumor suppressors, composed of five homologous proteins [25]. ING4 is present in multiple human tissues, and it is very often mutated in various cancers [26,27]: its decreased expression and dysregulation is widely observed in the latter [28]. In fact, ING4 plays a key role in cell cycle arrest, autophagy, apoptosis, hypoxic adaptation, cell contact inhibition, cell invasion, metastasis, and tumor angiogenesis. These features are associated with regulation of: (i) the chromatin acetylation of H3 by the histone acetyl transferase complex HBO1; and, (ii) the transcriptional activity of p53 and NF-κB. The structure of ING4 [27,29–33] consists of a folded antiparallel coiled-coil domain at its N-terminal region, and a folded plant homeodomain finger at its C-terminus (which is used for binding to the trimethylated histone H3 at Lys4) connected by an 85-residue-long disordered, basic region, with a bipartite nuclear localization signal (NLS) and an additional basic cluster ($R^{142}ARSK^{146}$), which is used in the binding to p53 [34].

Nuclear translocation generally occurs through specific carrier proteins called importins, being helped by other auxiliary proteins [35,36]. The most commonly described nuclear import pathway is activated by the recognition of an NLS in the cargo (protein) by importin α [37]. The complex formed between the cargo and importin α binds to importin β, and the ternary complex goes through the nuclear pore complex (NPC). Importin α is a modular protein, having several α-helix armadillo (ARM) repeat units [35,36]. It contains three regions: (i) an N-terminal importin β-binding (IBB) domain, which mediates binding to importin β before transport through the NPC; (ii) a well-folded NLS-binding domain formed by ten ARM units, which constitutes the main region of the protein; and, (iii) a short and disordered C-terminal region, which is often considered as a part of the main NLS-binding domain. In the absence of importin β, the IBB binds to the ARM units involved in NLS recognition [37]. Among other importins, we have considered Impα3 as a prototype carrier due to its larger flexibility compared with other isoforms, facilitating its interaction with various cargos [38]. In addition, Impα3 can be considered a model protein to investigate how the NLS sequence of the cargo can affect the thermodynamics of the binding; in fact, we have already carried out several studies of the binding of Impα3 and its truncated species, ΔImpα3 (without the IBB), to other NLSs [18,39–41].

Since the NLS region of ING4 is the binding region for p53, and it is also a substrate of PADI4 [42], we wondered whether: (i) the isolated wild-type region, encompassing the NLS, could also be a substrate of PADI4; (ii) an increased degree of citrullination of the NLS could affect the binding to PADI4; and (iii) the same degree of citrullination could alter the binding to either Impα3 or ΔImpα3. To answer those questions, we synthesized eight peptides corresponding to the wild-type NLS and its seven PTMs (with single, double and triple citrullination at positions Arg132, Arg142 and Arg144). We first characterized the conformational features of these isolated peptides by diffusion ordered spectroscopy (DOSY), 1D- and 2D-^{1}H NMR, and we found that all of them were disordered and monomeric in aqueous solution. To assess peptide binding to PADI4, Impα3 and ΔImpα3 we used fluo-

rescence, isothermal titration calorimetry (ITC) and biolayer interferometry (BLI). Whereas the first technique did not yield realistic values for the association constants, and ITC did not produce any measurable heat in the binding reaction with PADI4 for most of the peptides, BLI showed binding for all peptides to each protein. Furthermore, the wild-type peptide, ING-wt, was citrullinated by PADI4 and, therefore, it gave us a direct proof that it targets the active site of the enzyme. There were no relevant differences in the measured affinities for each of the three proteins among the three single citrulline PTMs, or, similarly, among the three double citrulline ones; in contrast, the triple citrulline PTM had the lowest affinities for each of the three proteins. Although, in general terms there was a slightly larger affinity of the peptides for ΔImpα3 than for Impα3 (as measured by ITC and BLI), the differences were not very larger. Molecular simulations could reproduce the general trend observed in the experiments *in vitro*, and provided the additional information that all the peptides targeted the expected hot-spots in the two proteins (i.e., the major NLS binding site of Impα3 and the catalytic site for citrullination of PADI4). In general, we can conclude that successive citrullination of the NLS could interfere the binding to PADI4, Impα3 or ΔImpα3, and then, it could affect nuclear translocation.

Materials and Methods

Materials

Imidazole, Trizma base, DNase, Ni^{2+}-resin, glycerol, N- α-Benzoyl-L-arginine ethyl ester (BAEE), L-citrulline, 3-hydroxyimino 2-butanone (diacetyl monoxime), thiosemicarbazide (TSC), SO_4H_2 (98%), PO_4H_3 (85%), $NH_4Fe(SO_4)_2 \times 12$ H_2O, NaCl, antipyrine, SIGMAFAST protease inhibitor tablets, 3-(trimethylsilyl) propionic acid-2,2,3,3-$^2H_4$-sodium salt (TSP) and ultra-pure dioxane were purchased from Sigma (Madrid, Spain). The β-mercaptoethanol was from BioRad (Madrid, Spain). Ampicillin and isopropyl- β-D-1-thiogalactopyranoside were obtained from Apollo Scientific (Stockport, UK). Triton X-100, TCEP (tris (2-carboxyethyl)phosphine), GSK484 (Cayman Chemical), dialysis tubing with a molecular weight (MW) cut-off of 3500 Da, and the SDS protein marker (PAGEmark Tricolor) were from VWR (Barcelona, Spain). Amicon centrifugal devices with a MW cut-off of 30 or 50 kDa were from Millipore (Barcelona, Spain). The rest of materials were of analytical grade. Water was deionized and purified on a Millipore system.

Protein expression and purification

Impα3 and ΔImpα3 were purified as described before [43]. The dimeric protein PADI4 (with 663 residues *per* monomer) was also purified as previously described [11]. Protein concentrations were determined by ultraviolet (UV) absorbance, employing an extinction coefficient at 280 nm estimated from the number of tyrosines and tryptophans in both importin species (6 tyrosines and 6 tryptophans *per* monomer, $\varepsilon_{280\ nm}$ = 41,820 M^{-1} cm^{-1}) and PADI4 (10 tryptophans and 13 tyrosines *per* monomer, $\varepsilon_{280\ nm}$ = 73,540 M^{-1} cm^{-1}) [44].

Synthesis of the wild-type and citrullinated variants of the NLS of ING4

Based on previous results of the citrullination of the NLS of full-length ING4 [42], we devised the so-called ING peptides for the present study (Table 1). They were eight peptides, based on the 23-residue-long fragment Lys130-Glu152 of wild-type, full-length ING4, and encompassing all possible permutations of citrullination (i.e., the PTM was either present or absent) in correspondence with the three residues Arg133, Arg142, and Arg144. All peptides were soluble and they did not show any tendency to precipitate at the concentrations used in the NMR experiments. All of them were synthesized as acetylated and amidated peptides, to avoid possible structural fraying at both termini. We added in all of them a tyrosine at the C-terminal end to allow for the quantitative determination of their amount used by employing UV absorption at 280 nm [44]. A possible influence of the appended C-terminal tyrosine to the affinity values (measured either by ITC or BLI) has not been experimentally ruled out. However, a distinct (i.e., systematic rather than aspecific) contribution would require that this terminal residue be ordered and part of the core anchoring motif in the bound peptide, which seems unlikely due to its peripheral location and the disordered-prone nature of each peptide in solution (see Results section). The ING peptides were produced by GenScript (Leiden, Netherlands), with a purity larger than 95%.

Fluorescence

For the titration of PADI4, Impα3 or ΔImpα3 with the ING peptides, increasing concentrations of the latter, in the range 0–30 μM, were added to a solution with a fixed amount of each of those proteins (3 μM in protomer units). Experiments were carried out at pH 8.0 (50 mM, Tris buffer) and 25 °C. The samples were excited at 280 and 295 nm, and the experimental set-up has been described in detail elsewhere [45]. In all cases, the appropriate blank corrections were subtracted. Spectra were corrected for inner-filter effects during fluorescence excitation [46].

We attempted to calculate the dissociation constant for each complex, K_d, by fitting the binding isotherm constructed by plotting the observed fluorescence change as a function of peptide concentration to the general binding

Table 1 Hydrodynamic properties of the ING peptides.[a]

ING peptide from ING4	D ($cm^2\ s^{-1}$) (R_h, Å)[b]	R_h, Å[c]
K^{130}KGRTQKEKKAARARSKGKNSDE^{152}Y (ING-wt)	$(1.62 \pm 0.01) \times 10^{-6}$ (15 ± 1)	14 ± 2
K^{130}KG**Cit**TQKEKKAARARSKGKNSDE^{152}Y (ING-mut1)	$(1.82 \pm 0.05) \times 10^{-6}$ (13 ± 2)	14 ± 2
K^{130}KGRTQKEKKAA**Cit**ARSKGKNSDE^{152}Y (ING-mut2)	$(1.95 \pm 0.08) \times 10^{-6}$ (12 ± 2)	14 ± 2
K^{130}KGRTQKEKKAARA**Cit**SKGKNSDE^{152}Y (ING-mut3)	$(1.9 \pm 0.1) \times 10^{-6}$ (12 ± 3)	14 ± 2
K^{130}KG**Cit**TQKEKKAA**Cit**ARSKGKNSDE^{152}Y (ING-dmut1)	$(2.1 \pm 0.2) \times 10^{-6}$ (13 ± 3)	14 ± 2
K^{130}KG**Cit**TQKEKKAARA**Cit**SKGKNSDE^{152}Y (ING-dmut2)	$(2.1 \pm 0.2) \times 10^{-6}$ (14 ± 3)	14 ± 2
K^{130}KGRTQKEKKAA**Cit**A**Cit**SKGKNSDE^{152}Y (ING-dmut3)	$(1.92 \pm 0.04) \times 10^{-7}$ (14 ± 2)	14 ± 2
K^{130}KG**Cit**TQKEKKAA**Cit**A**Cit**SKGKNSDE^{152}Y (ING-tmut)	$(2.00 \pm 0.08) \times 10^{-6}$ (14 ± 2)	14 ± 2

[a] All the peptides were amidated at their C-termini, and acetylated at their N-termini. The MW for the ING-wt is 2765.1 Da. The modified citrullines are indicated in bold.
[b] The R_h was determined by using the translational diffusion coefficient of dioxane, R_h, of 2.12 Å [51] and the Stokes-Einstein equation. Errors in D are fitting errors to an exponential curve and errors in R_h are due to propagation errors in the calculation [51].
[c] Calculated from the scale law: $R_h = (0.027 \pm 0.01)\ MW^{(0.50 \pm 0.01)}$ [78], where MW is the molecular weight of the peptide. Errors are due to propagation errors resulting from the equation used. The difference in MW between the wild-type species and each citrulline variant is 1 Da *per* introduced citrulline.

model, explicitly considering peptide depletion due to the binding [47,48]:

$$F = F_0 + \frac{\Delta F_{max}}{2[P]_T}\left(([P]_T + [Pep]_T + K_d) - \sqrt{\left(([P]_T + [Pep]_T + K_d)^2 - 4[P]_T[Pep]_T\right)}\right) \quad (1)$$

where F is the measured fluorescence at any particular concentration of each ING peptide after subtraction of the corresponding blank; ΔF_{max} is the largest change in the fluorescence of the ING peptide when all polypeptide molecules were forming the complex, taking as reference the fluorescence of each isolated chain; F_0 is the fluorescence intensity when no ING peptide was added; $[Pep]_T$ is the total concentration of the peptide, that was varied during the titration; and $[P]_T$ is the constant concentration of PADI4, Impα3, or ΔImpα3. Each titration (PADI4, Impα3 or ΔImpα3 with an ING peptide) was repeated three times, using newly prepared samples. In all cases, the variations in the results were lower than 10%. Fitting to Eq. (1) was carried out by using KaleidaGraph version 3.5 (Synergy software, Reading, PA, USA).

Nuclear magnetic resonance (NMR)

The NMR experiments of the ING peptides were performed at 10 °C on a Bruker Avance 500 MHz spectrometer (Bruker GmbH, Karlsruhe, Germany), equipped with a triple resonance probe and z-pulse field gradients. Spectra were processed with Bruker TopSpin 2.1 (Bruker GmbH, Karlsruhe, Germany). All NMR experiments were carried out in 50 mM sodium phosphate buffer, at pH 7.2, in the presence of 50 μL of D_2O. Spectra were calibrated with TSP, by considering pH-dependent changes of its chemical shifts [49]; probe temperature was calibrated with methanol [49].

1D-^{1}H NMR spectra. A number of 128 scans were acquired with 16 K acquisition points for the homonuclear 1D-^{1}H NMR spectra of each isolated ING peptide at ∼1.2 mM concentration. Water signal was suppressed with the WATERGATE sequence [50]. The spectra were processed after zero-filling (up to 32 K), apodised with an exponential window and base-line corrected.

Translational diffusion NMR (DOSY). The peptide concentrations in DOSY experiments were ∼100 μM, and 128 scans were acquired, with a total amount of data of 16 K in the F_2 dimension. Measurements of the translational self-diffusion coefficient, D, were performed with the pulsed-gradient spin-echo sequence in the presence of 100% D_2O. Details on the experimental conditions, calibration of the gradient strength and fitting of the resulting curves have been described elsewhere [45]. A final concentration of 1% of dioxane, which was assumed to have a hydrodynamic radius R_h of 2.12 Å [51], was added to the solution to estimate the D of the peptides in solution.

2D-^{1}H NMR spectra. Two-dimensional spectra of the eight ING peptides were acquired in each dimension in phase-sensitive mode by using the time-proportional phase incrementation technique [52] and a spectral width of 5500 Hz; peptide concentration was the same used in the 1D-^{1}H NMR spectra. Standard TOCSY (with a mixing time of 80 ms) [53] and NOESY experiments (with a mixing time of 250 ms) [54] were performed by acquiring a data matrix size of 4096 × 512 points. The DIPSI (decoupling in the presence of scalar interactions) spin-lock sequence [55] was used in the TOCSY experiments with a relaxation time of 1 s. A number of 96 scans were acquired *per* increment in the first dimension. NOESY spectra were collected with 128 scans *per* increment in the first dimension with a relaxation time of 1 s. In both spectra, residual water signal was removed by using the WATERGATE sequence [50]. Data were zero-filled, resolution-enhanced with a square sine-bell window function

optimized in each spectrum, and baseline-corrected. The ^{1}H resonances were assigned by using the standard sequential assignment method [56]. The chemical shift values of H_α protons in random-coils were obtained taking into account neighboring residue effects [56–58].

Isothermal titration calorimetry (ITC)

The binding affinities for the ING peptides interacting with PADI4, Impα3 or ΔImpα3 were determined in a high-sensitivity Auto-iTC200 calorimeter or PEAQ-ITC calorimeter (MicroCal, Malvern-Panalytical, Malvern, UK). The titrations were carried out in phosphate buffer (pH 8.0, 50 mM). Protein solutions in the cell at 10–15 μM were titrated with the ING peptide solutions at 100–200 μM from the injection syringe. In each experiment a sequence of nineteen injections of 2 μL of titrant solution spaced evenly over 150 s was programmed, with a stirring speed of 750 rpm and a reference power of 10 μcal/s. Experiments were repeated twice.

Data analysis was performed by applying the single ligand binding site model [59]. Briefly, the concentration of peptide and protein inside the calorimetric cell after each injection j were calculated as follows:

$$[Pep]_{T,j} = [Pep]_{syr}\left(1 - \prod_{k=1}^{j}\left(1 - \frac{v_k}{V_0}\right)\right)$$
$$[P]_{T,j} = [P]_{cell}\prod_{k=1}^{j}\left(1 - \frac{v_k}{V_0}\right) \quad (2)$$

where $[Pep]_{syr}$ is the concentration of peptide in the syringe, $[P]_{cell}$ is the initial concentration of protein in the cell, v_k is the volume of each injection, V_0 is the cell volume, and j is the injection number. A factor n multiplying $[P]_{cell}$ was included in Eq. (2) to account for a fraction of non-binding-competent protein in the calorimetric cell. The concentration of complex P:Pep after each injection was calculated by using the following expression, which is obtained when solving the chemical equilibrium for the formation of the complex:

$$[P:Pep] = \frac{1 + K_a[P]_T + K_a[Pep]_T - \sqrt{\left(1 + K_a[P]_T + K_a[Pep]_T\right)^2 - 4K_a^2[P]_T[Pep]_T}}{2K_a} \quad (3)$$

The binding isotherm (ligand-normalized injection heats as a function of the molar ratio) was built by integrating the injection heat effects recorded in the thermogram (thermal power as a function of time), and the theoretical heat effect was calculated as follows:

$$Q_j = \frac{1}{v_j[L]_{syr}}V_0\Delta H\left([P:Pep]_j - [P:Pep]_{j-1}\left(1 - \frac{v_j}{V_0}\right)\right) + Q_d \quad (4)$$

where $[P$:$Pep]_j$ is the concentration of complex formed after injection j (calculated with Eq. (3)) and Q_d is the background injection heat (usually called “dilution heat”, but it includes many other unspecific phenomena such as mechanical mixing and buffer neutralization). The equilibrium association constant, K_a (and the dissociation constant, $K_d = 1/K_a$), and the apparent binding stoichiometry, n, were estimated through non-linear least squares regression analysis of the data performed in Origin 7.0 (OriginLab, Northampton, MA, USA).

Citrulline determination by a colorimetric assay

A photometric method was carried out to determine whether PADI4 was capable of citrullinating BAEE (as a control), or alternatively, the peptide ING-wt. This method is based in the reaction of citrulline with oximes in strong acids in the presence of TSC. The protocol to prepare the color developed reagent (COLDER) and the corresponding tests have been described elsewhere [60] and applied to detect the enzymatic activity of PADI4 under different conditions [21,60,61]. For monitoring the citrullination, we also used the modification of the COLDER reaction in the presence of antipyrine [62,63], which yields a yellow-colored compound instead of a red-pink one.

To test the citrullination of isolated peptide ING-wt, we used the same procedure and protocols described elsewhere for other assayed peptides [21]. All the controls and the reactions were made in duplicate for each of the colorimetric reagents (COLDER alone or with antipyrine). The control experiments were performed in tubes containing: (i) 100 μM of isolated L-citrulline; (ii) only the reaction buffer; (iii) BAEE (100 μM); and (iv) 100 μM of GSK484 (an inhibitor of the enzyme) and BAEE (100 μM). The reaction buffer in all cases contained 100 mM Tris (pH 7.6), 50 mM NaCl, 2 mM DTT and 10 mM $CaCl_2$ up to a final volume of 500 μL. To the tubes containing the reaction buffer except the ones containing only this buffer, and that with L-citrulline we added PADI4 from a stock solution, to yield a final concentration of 0.75 μM (in protomer units). Next, we added a volume from a stock solution of peptide ING-wt to yield a final concentration of 100 μM in the tubes testing its ability to be citrullinated. An identical volume of water was added to the other test solutions. The resulting solutions were incubated for 25 min at 37 °C in an Innova 4000 New Brunswick Scientific incubator (ThermoFisher, Madrid, Spain) with a stirring speed of 190 rpm.

All samples were incubated at 37 °C for 25 min in the same shaker under agitation. Reactions were quenched by flash freezing the tubes in liquid nitrogen. For color development, 2 mL of freshly prepared COLDER solution were added to the quenched reaction, vortexed to ensure complete mixing, and incubated for 15 min at 95 °C; the same amount of reagent containing antipyrine was added to the other tubes in parallel. After cooling at room temperature, the samples were

transferred into 1 mL-quartz cuvettes to acquire their UV absorption spectra. All these spectra were recorded between 400 and 600 nm on an UV–Visible spectrophotometer Shimadzu UV-1603 by Shimadzu (Kyoto, Japan) at room temperature. Water was used for the blank subtraction.

Biolayer interferometry (BLI)

Experimental design. The association (k_{on}) and dissociation (k_{off}) rate constants of the binding of the ING peptides to PADI4, Impα3 or ΔImpα3 were determined by using a BLItz system (ForteBio, Pall, Barcelona, Spain) [64–68]. The buffer used in the experiments was that recommended by the manufacturer (Octet kinetics Buffer 10 × (10 × KB), PN 18-1105, Sartorius). As PADI4, Impα3, and ΔImpα3 had a His-tag, they were immobilized on His-tag biosensors (Octet NTA Biosensors, PN 18-5101) at 0.3 μM (in protomer units). Before the loading, each ING peptide was tested for binding at the largest concentration assayed against unloaded tips; in all the cases, we did not observe any binding. The ING peptide concentrations were in the range from 1 to 20 μM during the association step. The general scheme of the protein-association/dissociation reactions was: 30 s of initial baseline acquisition with the 10 × kinetics buffer; 120 s of loading PADI4, Impα3 or ΔImpα3 into the His-tag biosensor; 30 s of baseline acquisition with the 10 × kinetics buffer; 120 s of association of each ING peptide to the biosensor-immobilized-PADI4/Impα3/ΔImpα3; and 120 s of dissociation of the ING peptide from the biosensor-immobilized-PADI4/Impα3/ΔImpα3. Baseline measurements in the presence of unloaded tips were subtracted from their matched measurement taken with the loaded tip. Experiments were repeated twice with new biosensors.

Fitting of the sensorgrams. Fitting of the sensorgrams was carried out as described elsewhere [64–68]. The experimentally interferometry response during the association step, $R(t)$, after loading the biosensor with PADI4, Impα3 or ΔImpα3 was fitted as:

$$R(t) = R_{eq} - R_{eq} e^{(-k_{obs}\ (t-t_0))} - R'_{eq}(\ t - t_0) \quad (5)$$

where the last term was included to consider the linear drift observed at longer times. In this equation, the R_{eq} is the steady-state (or equilibrium) response obtained at infinite time, when $dR(t)/dt = 0$, and $t_0 = 180$ s is the time at which the association step started. The value of k_{obs} obtained at different peptide concentrations is given by the pseudo-first-order equation:

$$k_{obs} = k_{on}[Pep] + k_{off} \quad (6)$$

where the k_{on} and k_{off} are, respectively, the kinetic association and dissociation rates of the binding reaction of the corresponding ING peptide to each of the proteins.

The dissociation process was fitted with $R(t)$ given by:

$$R(t) = R_2 - R_1\ e^{(-k_{off}(t-t_0))} - R''_{eq}(\ t - t_0) \quad (7)$$

where $t_0 = 300$ is the time at which the dissociation of the peptide from the biosensor-bound-PADI4/Impα3/ΔImpα3 started in our experimental set-up, R_1 is the response level when dissociation starts, R_2 is the response at infinite time values, and the last term, R''_{eq}, was included to consider the linear drift observed at longer times. Separated fittings of the association and the dissociation steps to Eqs. (5) and (7), at the different peptide concentrations for each protein target, were carried out by using KaleidaGraph. Fitting to Eq. (6) (the so-called pseudo-first-order plot) was carried out also with KaleidaGraph.

Molecular docking simulations

Molecular docking simulations were performed to investigate the binding locations of the ING peptides on both Impα3 and PADI4. Impα3 was modeled on the basis of its crystallographic complex with the NLS of the Ran-binding protein 3 deposited in the Protein Data Bank (PDB entry: 5XZX [69]. The structure of Impα3 was considered without both the N-terminal IBB domain (which inhibits the anchoring of any other molecular partner when self-bound to the protein, or is otherwise disordered and little relevant for the binding when displaced in the solvent) and the C-terminal region (which is short and also disordered). PADI4 was modeled on the basis of its crystallographic structure (PDB entry: 3APN [70]) and included all its missing loop regions, reconstructed *in silico* as previously described [11]. The ING peptides were modeled by using UCFS Chimera [71], and included cappings at their N and C termini (acetylated and methylated, respectively).

The large conformational flexibility (117 rotatable dihedral angles) of the ING peptides did not allow us to use most traditional docking software. Therefore, the molecular docking algorithm DiffDock was employed, which relies on a diffusion generative model based on deep learning [72]. Computational parameters were similar to those we previously used to simulate the binding of other peptides to Impα3 and to PADI4 [21,73]: twenty diffusion time divisions, eighteen actual inference steps, and no final step noise applied. In all cases, blind docking simulations were performed starting from the ING peptides in a fully extended conformation. Local steric clashes or small distortions (i.e., deviations from the ideal bond angle values in aliphatic side-chains) in the output conformations were relaxed by a short (100 steps) energy minimization using the steepest descent algorithm with the GAFF force field [74]. The final docking poses obtained were

visualized by using the molecular software VMD, version 1.9.3 [75].

Bioinformatic analysis of the peptide sequences

The bioinformatic analysis tool CIDER (Classification of Intrinsically Disordered Ensemble Regions) was used to analyze the peptide sequences [76]. CIDER calculates parameters such as the fraction of charged residues (FCR), net charge per residue (NCPR), and charge segregation (κ), using as input the sequence in FASTA format. Since the website of CIDER does not allow the introduction of citrulline residues, we substituted in the input a glutamine instead of each citrulline for the ING peptides with this PTM. In fact, the side-chains of these two amino acids are similar in terms of their physico-chemical properties, at least for those of our interest in this analysis.

Results

Conformational features of the ING peptides

To perform the characterization of the conformational features of the ING peptides (Table 1), we carried out 1D- and 2D-^{1}H NMR studies. We did not use fluorescence to characterize the structural features of the isolated peptides, since all of them had a non-natural tyrosine at the C-terminal region, to allow for measurement of their concentration. Furthermore, the position of the maximum wavelength of tyrosine residues does not change significantly with its environment [77].

The ING peptides were monomeric, as concluded from: (i) the value of D measured by the DOSY experiment (Table 1); and (ii) the estimated R_h obtained from the comparison with the experimentally measured D of dioxane by using the Stokes-Einstein relationship [51]. The estimated values of R_h were similar to those obtained theoretically for random-coil polypeptides [78] with the same MWs (Table 1).

The disordered character of the ING peptides was indicated by the 1D-^{1}H NMR spectra (Figure 1 and Figure S1), which showed a clustering of all the methyl protons of alanine around 1.4 ppm. In the ING peptides, we could not rely on the presence of methyl groups belonging to Leu, Val or Ile, between 0.8 and 1.0 ppm in random-coil environments [56], because the peptide sequences do not contain such residues (Tables ST1–ST8). Similarly, the amide protons were clustered between 8.0 and 8.6 ppm in all peptides (Figures S2 and S3). These values for alanine methyls and amide protons are typical of residues belonging to disordered chains [56].

To further confirm the disordered nature of the ING peptides, we also carried out 2D-^{1}H NMR experiments (Tables ST1–ST4). The peptides

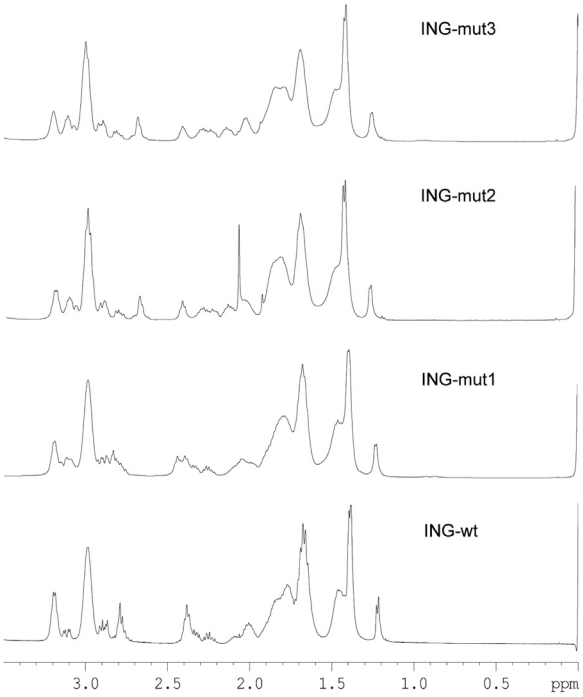

Figure 1. Conformational features of isolated ING peptides in solution as measured by 1D ^{1}H NMR: Methyl regions of the 1D-^{1}H NMR spectra of some of the isolated ING peptides. The signal appearing at 0 ppm is that of TSP. Spectra were acquired at 10 °C and pH 7.2 (50 mM, sodium phosphate buffer).

were mainly disordered in solution, as suggested by two pieces of evidence. First, the sequence-corrected conformational shifts ($\Delta\delta$) of H_α protons [56–58] for unambiguously assigned residues were within the commonly accepted range for random-coil peptides ($\Delta\delta \leq 0.1$ ppm) (Tables ST1–ST8). And second, no long- or medium-range NOEs were detected, but only sequential ones (i.e., αN (i, $i+1$) and βN (i, $i+1$)) in the polypeptide patches fully assigned (Figure 2). It is interesting to note that the successive citrullination did not affect the chemical shifts of backbone or side-chain protons (Tables ST1–ST8).

Therefore, we can conclude that all isolated ING peptides in solution were monomers with a disordered conformation.

ING peptides were capable of binding to Impα3 and ΔImpα3

We carried out fluorescence titrations to determine the affinity constant towards Impα3 and ΔImpα3, fixing the concentration of each of the importin species, and raising that of the corresponding ING peptide. We also used ITC to determine the affinity constant. And, finally, we used BLI to determine the kinetic parameters of the binding reactions, and to estimate an affinity constant of the reaction (to compare with those

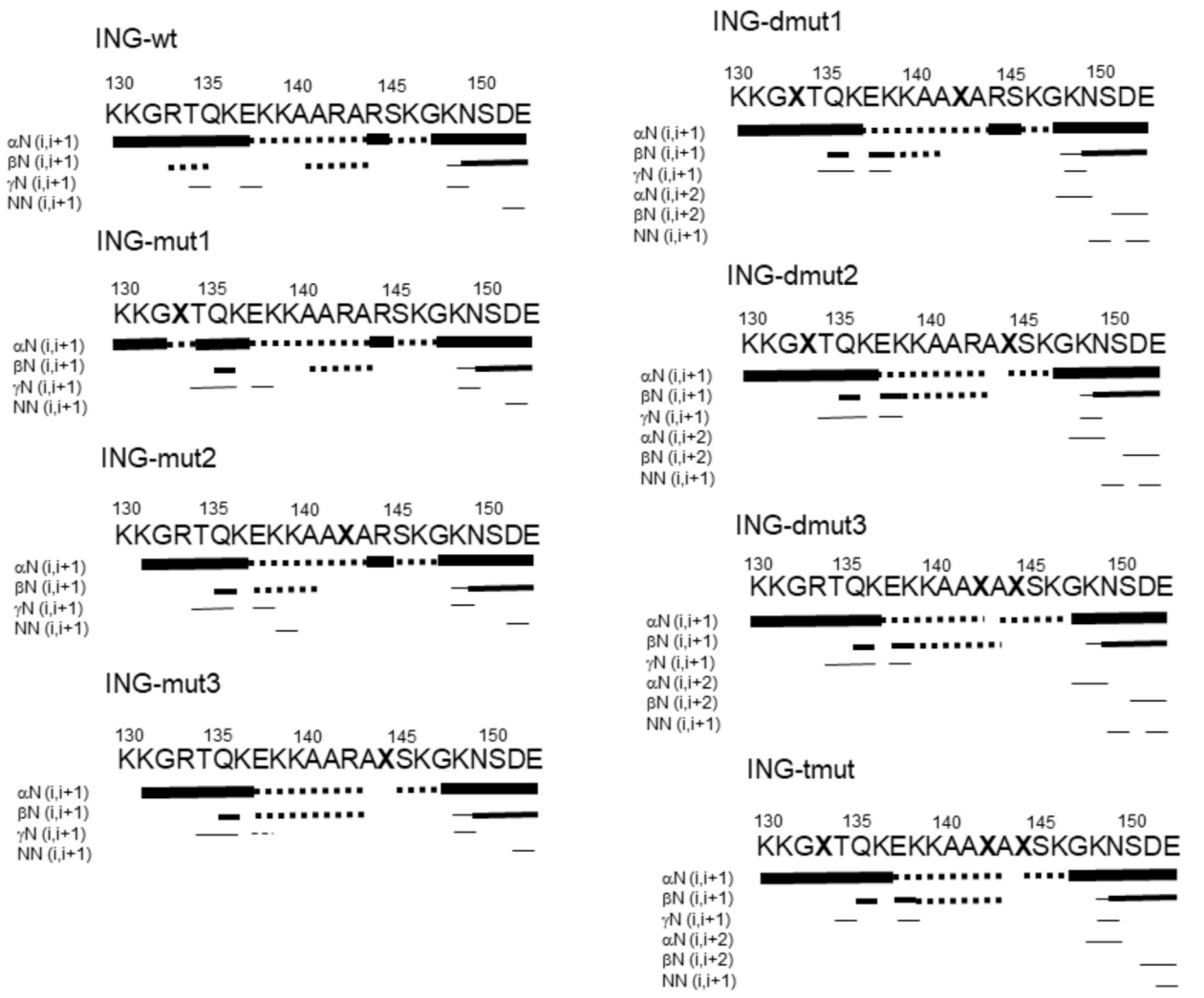

Figure 2. NOE diagrams of the isolated ING peptides in aqueous solution from the 2D-^{1}H NMR NOESY spectra: NOEs are classified as strong, medium or weak, and represented by the height of the bar underneath the sequence; signal intensity was judged from the NOESY experiments. The dotted lines indicate NOE contacts that could not be unambiguously assigned due to signal overlapping.

obtained by the other two techniques), assuming a two-state process for the binding of each peptide to the importin species. It is important to pinpoint that, in the context of the fluorescence experiments, we are also assuming that the unbound and the free species were the only ones significantly populated (Eq. (1)). However, in the context of the BLI experiments, if we assume that there are more than those two species (that is, an intermediate one exists between the free and bound states) the equilibrium dissociation constant cannot be obtained as $K_d = k_{off}/k_{on}$, but rather by using more complex relationships [79].

We first carried out fluorescence titrations with each of the eight peptides and either Impα3 or ΔImpα3. We observed a decrease of the fluorescence intensity as the concentration of the ING peptide was increased (by following the titration at either 280 or 295 nm) at any of the explored emission wavelengths; however, such variation could not be fitted to Eq. (1), and we were not able to determine a reliable K_d value for any peptide (Figure 3). In Figure 3, as representative titration curves, we have selected two peptides for each importin species; in these examples, the fluorescence spectra were obtained by excitation at either 280 or 295 nm, and the emission fluorescence were observed at 315 or 330 nm. In that way, we indicate that the titration behavior did not depend on: (i) the chosen peptide; (ii) the excitation wavelength used to acquire the spectra; or (iii) the emission wavelength chosen to monitor the binding. In spite of this, our results further suggest that, since all the ING peptides contained a tyrosine (Table 1), and we observed a decrease of the fluorescence after excitation at 295 nm (where only indole moieties are excited), the binding took place and

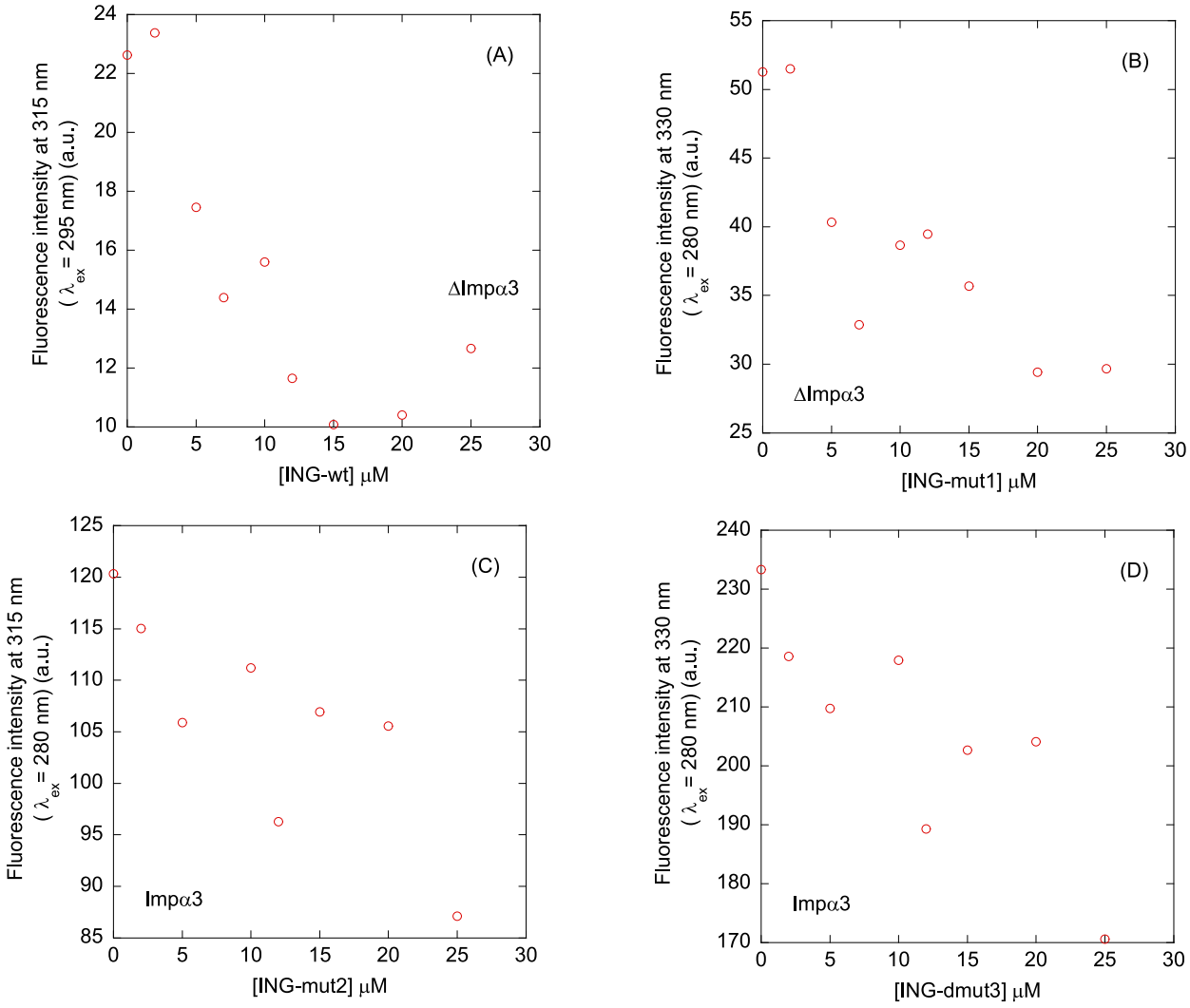

Figure 3. Fluorescence titration curves of selected ING peptides to either Impα3 or ΔImpα3: Titration curves of selected ING peptides with the importin species obtained by either excitation at 280 or 295 nm, observed at different wavelengths. All experiments were performed at 25 °C. Experiments were repeated three times.

involved at least some of the tryptophans of the importin species (six residues in each protein).

The calorimetric titrations with the ING peptides revealed that all of them were capable of binding to each importin species, Impα3 and ΔImpα3 (Figures 4 and S4). All the dissociation constants were in the low micromolar range (Table 2), with affinities decreasing as the number of citrulline residues in the peptide raised. Further, the affinities for ΔImpα3 were slightly higher than those for Impα3. A possible influence of the appended C-terminal tyrosine to the affinity values has not been experimentally ruled out. However, a distinct (i.e., systematic rather than aspecific) contribution would require that this terminal residue be ordered and part of the core anchoring motif in the bound peptide, which seems unlikely due to its peripheral location and the disordered-prone nature of each peptide in solution (see above, Section 'Conformational features of the ING peptides', and the findings *in silico*, Section 'ING peptides targeted the NLS binding site of importin species and the active site of PADI4').

Finally, we carried out BLI experiments to have another independent estimate of the apparent affinity of the binding of each ING peptide (Table 3, Figures 5 and Figure S5) to the importin species. It is important to indicate that due to the attachment of any of the importins to the biosensor, then some of the potential peptide-binding regions of the protein could get occluded, then hampering binding to the peptide. Although this is true and we acknowledge such limitation, which is a well-known drawback of the technique [64–67], in our case, we wanted to have an additional method to further confirm the binding of the peptides to the proteins in case that fluorescence

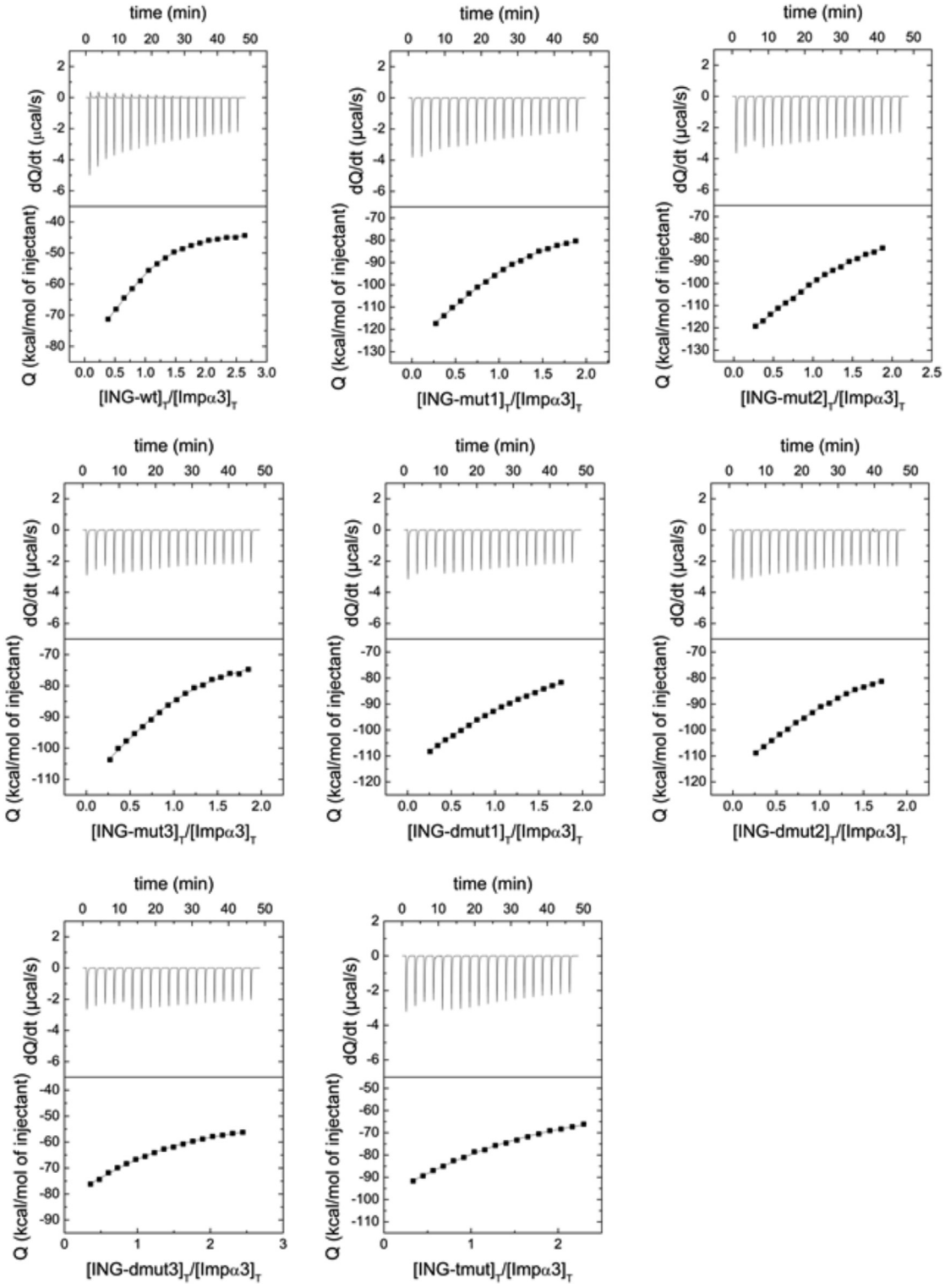

Figure 4. Quantitative determination of the binding of ING peptides to Impα3 as monitored by ITC: Calorimetric titrations of Impα3 with the eight ING peptides. Upper panels show the thermograms (thermal power as a function of time) and lower panels show the binding isotherms (ligand-normalized heat effects per injection as a function of the molar ratio in the calorimetric cell). Continuous curves correspond to the non-linear least-squares fittings according to a single ligand binding site interaction model. Experiments were carried out at 25 °C. Experiments were repeated twice.

Table 2 Thermodynamic parameters of the binding of the importin species to the ING peptides as determined by ITC.[a]

	Impα3			ΔImpα3		
	K_a (M^{-1})	K_d (μM)	n	K_a (M^{-1})	K_d (μM)	n
ING-wt	2.6×10^5	3.8	0.8	3.2×10^5	3.1	0.9
ING-mut1	1.9×10^5	5.3	0.9	4.0×10^5	2.5	0.7
ING-mut2	1.3×10^5	7.7	1.1	4.3×10^5	2.3	0.7
ING-mut3	1.6×10^5	6.3	0.8	2.2×10^5	4.5	0.9
ING-dmut1	0.80×10^5	13	1.2	1.3×10^5	7.7	0.8
ING-dmut2	1.2×10^5	8.3	1.0	1.3×10^5	7.7	0.7
ING-dmut3	0.76×10^5	13	1.0	1.2×10^5	8.3	0.9
ING-tmut	0.63×10^5	16	1.2	0.69×10^5	14	1.3

[a] Relative error in K_a and K_d is 30%, obtained from two measurements.

Table 3 Kinetic parameters of the binding of importin species to the ING peptides as determined by BLI.

	Impα3			ΔImpα3		
	k_{on} (μM^{-1} s^{-1})[a]	k_{off} (s^{-1})[b]	K_d (μM) (=k_{off}/k_{on})[c]	k_{on} (μM^{-1} s^{-1})[a]	k_{off} (s^{-1})[b]	K_d (μM) (=k_{off}/k_{on})[c]
ING-wt	0.0254 ± 0.0002	0.077 ± 0.001	3.0 ± 0.4	0.024 ± 0.004	0.073 ± 0.001	3.1 ± 0.8
ING-mut1	0.027 ± 0.005	0.078 ± 0.001	2.8 ± 0.7	0.022 ± 0.003	0.063 ± 0.001	2.9 ± 0.6
ING-mut2	0.015 ± 0.003	0.072 ± 0.002	4.7 ± 0.4	0.016 ± 0.002	0.065 ± 0.001	4.0 ± 0.5
ING-mut3	0.016 ± 0.002	0.061 ± 0.002	4.2 ± 0.3	0.020 ± 0.002	0.061 ± 0.001	3.0 ± 0.5
ING-dmut1	0.022 ± 0.003	0.092 ± 0.001	4.2 ± 0.9	0.016 ± 0.006	0.097 ± 0.002	6 ± 2
ING-dmut2	0.015 ± 0.003	0.081 ± 0.001	5.4 ± 0.8	0.014 ± 0.002	0.086 ± 0.001	6 ± 1
ING-dmut3	0.014 ± 0.003	0.088 ± 0.001	6 ± 1	0.021 ± 0.002	0.088 ± 0.001	4.0 ± 0.9
ING-tmut	0.013 ± 0.003	0.110 ± 0.001	8.6 ± 0.9	0.018 ± 0.002	0.14 ± 0.003	7 ± 1

[a] Obtained from pseudo-first order plots. Error for k_{on} is the fitting error to Eq. (6).
[b] The pseudo-first order plots had a negative y-axis intercept for: ING-mut2, ING-mut3, ING-dmut2 and ING-dmut3 (with Impα3); ING-wt, ING-mut1, ING-mut2, ING-mut3, ING-dmut2, ING-dmut3 and ING-tmut (with ΔImpα3). In this column, the average of all the k_{off} rates, obtained from the dissociation step of the sensorgrams for each concentration of the corresponding ING peptide, is shown (the error indicated is the standard deviation of the average value). The dissociation section of the sensorgrams was fit to Eq. (7).
[c] Errors are obtained from propagation errors for k_{on} and k_{off}. The estimation of the K_d is carried out assuming that the binding process was two-state [79].

(lack of changes around a tryptophan and/or tyrosine) or ITC (lack of an enough amount of heat exchanged) did not yield affinity constants. In general terms for ING peptides, the values of the k_{off} rates for both importin species were similar for all peptides, with a slight tendency to raise as the degree of citrullination increased (Table 3). In contrast, there was a general tendency observed for both importin species (although it was more clearly observed in Impα3) that, as the degree of citrullination increased, the value of the k_{on} rate for the binding reactions decreased. This means that the less arginine (positive) residues were present, the less favorable the binding rate was. As a consequence, as the degree of citrullination was increased, the affinity of the peptides was smaller (that is, larger value of the K_d). The k_{on} and k_{off} rates for the binding of each particular peptide to either Impα3 and ΔImpα3 were identical within the experimental error and, therefore, the apparent affinity K_d values were also similar, within the error, for both importin species according to BLI. We also note that, as in the case of the ITC results, a possible influence of the appended C-terminal tyrosine to the affinity values measured by BLI has not been ruled out, either (see above, Section 'Conformational features of the ING peptides', and the findings *in silico*, Section 'ING peptides targeted the NLS binding site of importin species and the active site of PADI4').

ING peptides were capable of binding to PADI4

As we had done with the ING peptides and the importin species, we carried out fluorescence titrations, ITC and BLI to determine the thermodynamic and kinetic parameters of the binding reaction of each of the eight ING peptides to PADI4.

In the fluorescence experiments, similarly to what was seen for importins, we observed a decrease of the fluorescence intensity as the concentration of each ING peptide was increased (either by following the titration at 280 or 295 nm); however, such variation could not be fitted to Eq. (1), and we were not able to determine a reliable K_d value of the binding to PADI4 for any peptide (Figure S6). In Figure S6, as representative titration curves, we have selected several peptides for which the fluorescence spectra were obtained by excitation at either 280 or 295 nm, and the emission fluorescence observed at 315 or 330 nm. In that way, we show that the titration behavior did not depend on: (i) the chosen peptide; (ii) the excitation wavelength used to

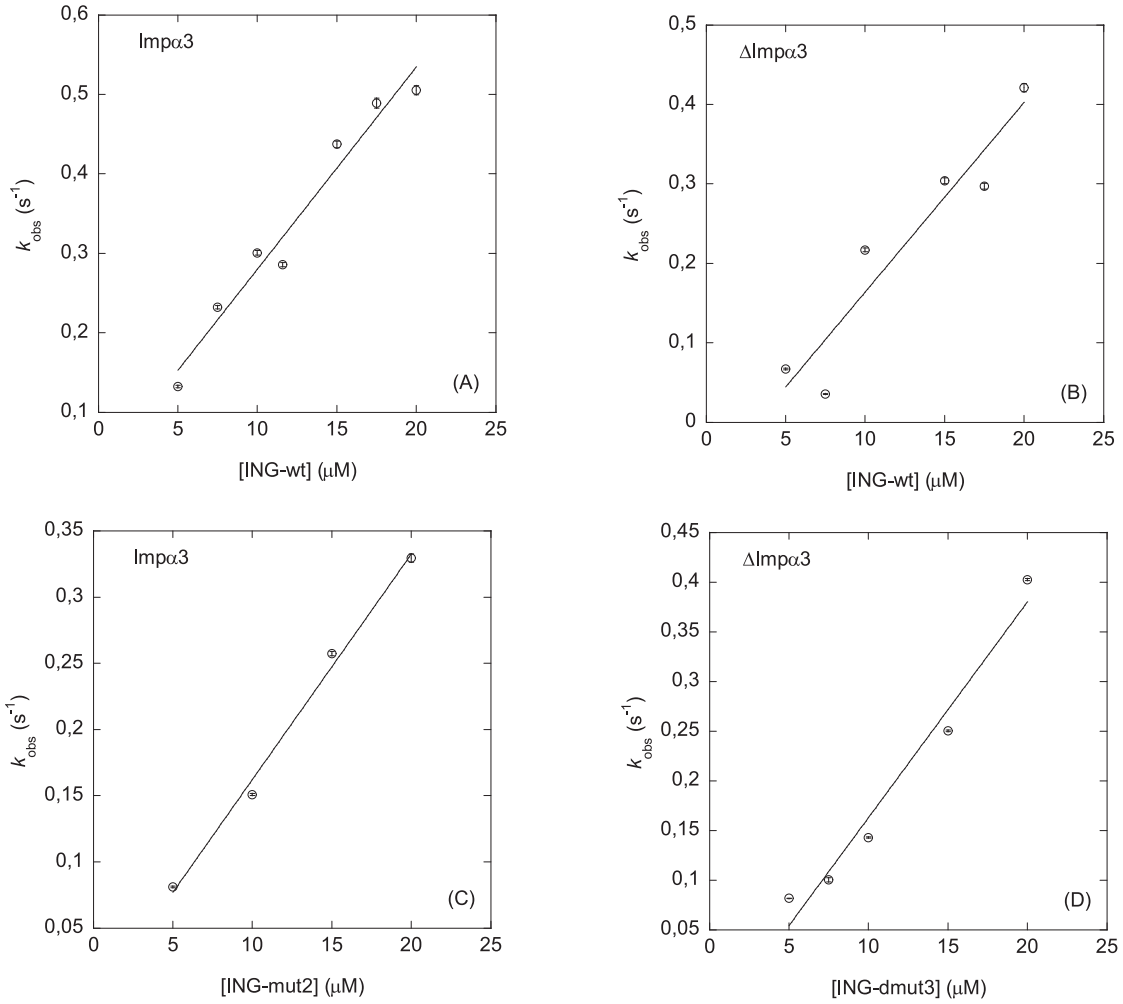

Figure 5. Binding of selected ING peptides to either Impα3 or ΔImpα3 as monitored by BLI: Pseudo-first-order plots of the binding of selected ING peptides to each of the importin species. The error bars of the fittings to Eq. (5) at each peptide concentration are indicated. Experiments were carried out at 25 °C. Experiments were repeated twice.

acquire the spectra; or (iii) the emission wavelength chosen to monitor the binding. Furthermore, our results suggest that, since all the ING peptides contained a tyrosine (Table 1), and we observed a decrease of the fluorescence after excitation at 295 nm (where only indole moieties are excited), the binding took place and involved at least some of the ten tryptophans of PADI4 (in each monomer).

When assessing the interaction of the ING peptides with PADI4 by using ITC, we could only determine the binding affinity for ING-wt (Figure 6), which was 1.3×10^5 M^{-1} for K_a (7.7 μM for K_d with an error of 30%) and an n value of 0.7. No interaction could be observed for peptides including any PTM, conversely to what happened with both importin species (Table 2). The binding affinity for ING-wt was also in the low micromolar range, similar to those affinities determined for importins.

Finally, we carried out BLI experiments to have another independent estimate of the affinity of the binding of the ING peptides to PADI4 (Figures S7 and S8), and in this technique, we measured the kinetic parameters of the binding for all peptides. In general terms, the values of the k_{off} rates were similar for all peptides, with a slight tendency to raise as the grade of citrullination increased. In contrast, as the grade of citrullination increased, the value of the k_{on} rate for the binding reactions to PADI4 decreased (Table 4, Figure S7). Thus, the more citrullines there were, the less favorable the rate of binding to the active site of the enzyme was. As a consequence, the larger the amount of citrulline residues in the peptide, the smaller the affinity, and then, the larger the K_d value. Therefore, the same trend for K_d values was observed for either importin species and PADI4, as measured by BLI. We can also conclude from

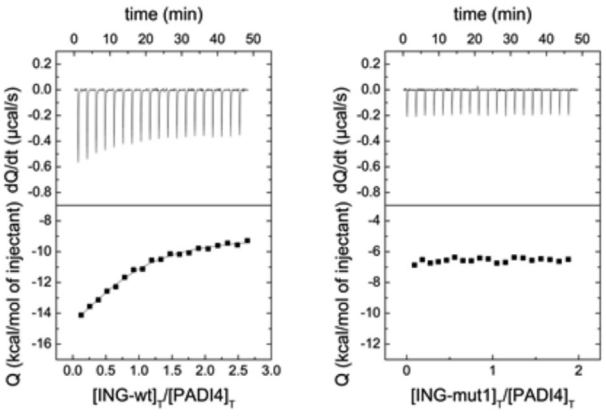

Figure 6. Quantitative determination of the binding of ING peptides to PADI4 as monitored by ITC: Calorimetric titrations of PADI4 with ING-wt and ING-mut1 (as a representative example). Upper panels show the thermograms (thermal power as a function of time) and lower panels show the binding isotherms (ligand-normalized heat effects per injection as a function of the molar ratio in the calorimetric cell). The continuous curve in ING-wt corresponds to the non-linear least-squares fitting according to a single ligand binding site interaction model. Experiments were carried out at 25 °C. Experiments were repeated twice.

the comparison of the rates in Tables 3 and 4 that: (i) the k_{off} rates were roughly the same for both importin species and PADI4 for each of the peptides, i.e. they were in the range 0.06–0.11 s^{-1}; (ii) for the k_{on} rates there was no similarity for the same peptide for the two importin species and PADI4 (being in the range 0.012–0.031 μM^{-1} s^{-1}).

Since, the affinity of the ING-wt peptide for PADI4 was the largest among the peptides, either measured by ITC (see above, Table 2) or BLI (Table 3), and such peptide does not contain any citrulline residue, we tested whether such peptide was capable of being citrullinated by PADI4. We observed that ING-wt was a substrate of the protein, since it was citrullinated in the presence of PADI4 (Figure S9), and therefore, we could conclude that it was bound to the active site of the enzyme.

ING peptides targeted the NLS binding site of importin species and the active site of PADI4

The *in vitro* techniques used to assess the binding of the ING peptides on both Impα3 and PADI4 could not provide details on the location of the protein hot-spots where they anchor, with the sole exception of the peptide ING-wt to PADI4 (Figure S9) (Section 'ING peptides were capable of binding to PADI4'). Structural techniques commonly used in biophysics, such crystallography and cryo-electron microscopy, are difficult to apply because of the difficulty in finding the conditions to form a complex stable enough due to the affinity constants measured for the complexes of the peptides with either PADI4 or the importin species (in the low-medium micromolar range, Tables 2–4). On the other hand, our NMR experiments could not be further pushed to clarify this point either, because identifying the binding hot-spot for both Impα3 and PADI4 would require a full-assignment of their resonances, which is practically unfeasible for proteins of this size. For this reason, we used molecular simulations to gain insights on the anchoring propensities of our peptides to the two proteins, with the help of the diffusion-based algorithm DiffDock [72].

Figures 7 and 8 show the results obtained in the molecular docking of the ING peptides on both Impα3 and PADI4. In particular, as evident in Figure 7, favorable docking poses for Impα3 were

Table 4 Kinetic parameters of the binding of PADI4 to the ING peptides as determined by BLI.

ING peptides	k_{on} (μM^{-1} s^{-1})[a]	k_{off} (s^{-1})[b]	K_d (μM) (=k_{off}/k_{on})[c]
ING-wt	0.032 ± 0.003	0.080 ± 0.001	2.5 ± 0.3
ING-mut1	0.029 ± 0.003	0.079 ± 0.001	2.8 ± 0.4
ING-mut2	0.029 ± 0.006	0.069 ± 0.002	2.4 ± 0.7
ING-mut3	0.012 ± 0.002	0.069 ± 0.001	6 ± 1
ING-dmut1	0.020 ± 0.004	0.102 ± 0.002	5 ± 2
ING-dmut2	0.008 ± 0.001	0.082 ± 0.001	10 ± 2
ING-dmut3	0.018 ± 0.003	0.075 ± 0.001	4 ± 1
ING-tmut	0.015 ± 0.004	0.109 ± 0.001	9 ± 4

[a] Obtained from pseudo-first order plots. Error for k_{on} is the fitting error to Eq. (6).

[b] The pseudo-first order plots yielded a negative *y*-axis intercept for: ING-wt, ING-mut2, ING-mut3 and ING-dmut3. Then, in this column, the average of all the k_{off} rates, obtained from the dissociation step of the sensorgrams for each concentration of the corresponding ING peptide, is shown (the error is the standard deviation of the average). The dissociation segment of the sensorgrams was fit to Eq. (7).

[c] Errors are obtained from propagation errors for k_{on} and k_{off}. The value of the K_d is obtained by assuming that the binding was two-state [79].

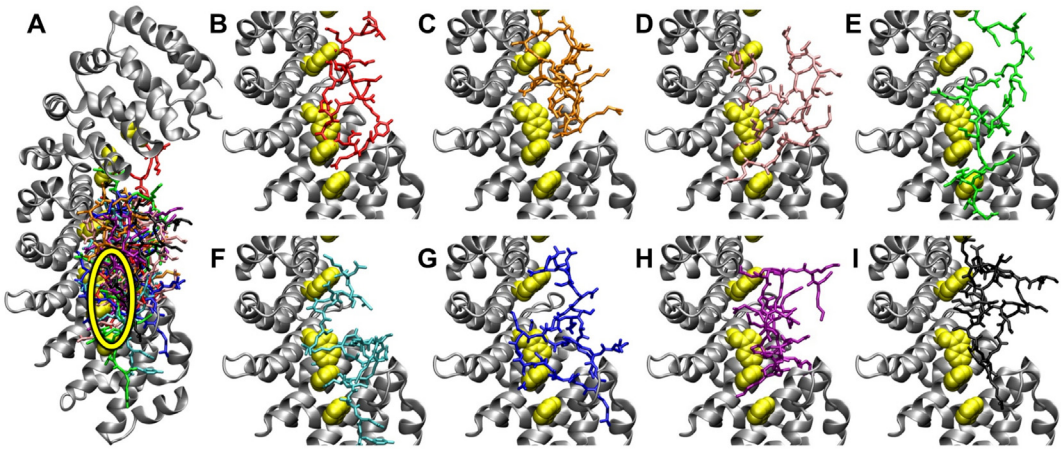

Figure 7. Docking poses of the ING peptides to Impα3 obtained in molecular simulations: (A) Impα3 is shown in ribbon structure (gray), with the major NLS binding site (circled in yellow), and Trp residues explicitly shown (van der Waals representation, atoms in yellow). The peptides are indicated: ING-wt (red), ING-mut1 (orange), ING-mut2 (pink), ING-mut3 (green), ING-dmut1 (cyan), ING-dmut2 (blue), ING-dmut3 (purple), ING-tmut (black). Details of each docking pose are given in panels (B)–(I).

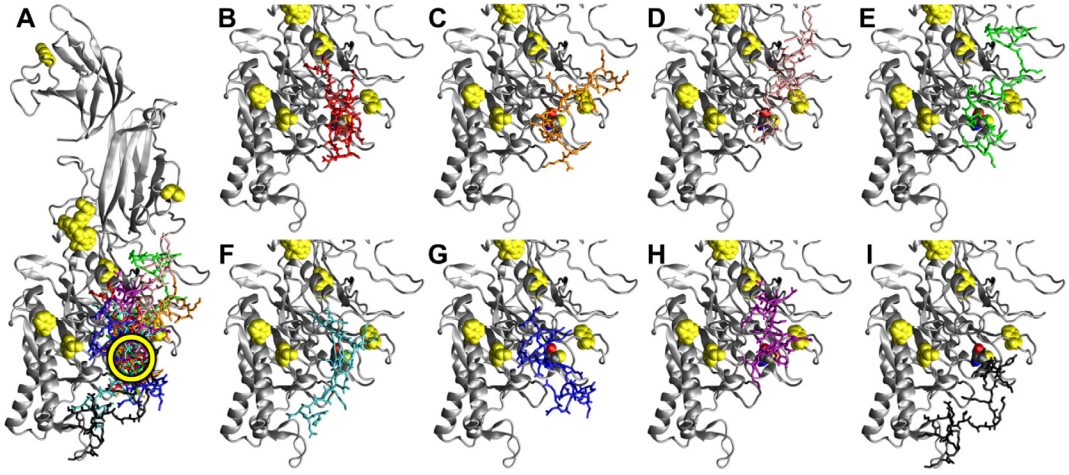

Figure 8. Docking poses of the ING peptides to PADI4 obtained in molecular simulations: (A) PADI4 is shown in ribbon structure (gray), with the active site (circled in yellow) containing the catalytic residue Cys645 (van der Waals representation, atoms colored by type) and Trp residues explicitly shown (yellow). The peptides are indicated: ING-wt (red), ING-mut1 (orange), ING-mut2 (pink), ING-mut3 (green), ING-dmut1 (cyan), ING-dmut2 (blue), ING-dmut3 (purple), ING-tmut (black). Details of each docking pose are given in panels (B)–(I).

found in correspondence with tryptophan residues, especially Trp137, Trp222, and Trp264. This finding agrees with our fluorescence experiments (Section 'ING peptides were capable of binding to Impα3 and ΔImpα3'), in which we observed a decreased in the fluorescence after excitation at 295 nm, where the indole moiety emits (Figure 3). These amino acid residues are located in the core region of the major NLS binding site of Impα3, and are crucial for the anchoring of cargo proteins. Other less favorable docking poses were invariably found in correspondence with (or adjacent to) both the major and minor NLS binding sites of Impα3 (data not shown), all along the sagittal plane of the inner concave surface of the folded protein domain. In the case of PADI4, as shown in Figure 8, top favorable docking poses for all the ING peptide species were found close to the key catalytic residue Cys645, which is responsible for the arginine-to-citrulline PTM. This hot-spot region contains a few nearby partly-exposed tryptophan residues in proximity to Cys645 (i.e., Trp347 at <1 nm), which could explain at least in part the decrease in the fluorescence after excitation at 295 nm (Figure S6). In the case of PADI4, however, we observed other less favorable docking poses scattered over several other regions of the surface

(data not shown), indicating a greater difficulty of the DiffDock search algorithm to identify the correct binding hot-spot.

The confidence score of DiffDock (dimensionless and with arbitrary units) for the most favorable docking poses of each peptide species interacting with Impα3 were in the range −3.7 ± 0.2, whereas for PADI4 they were −3.7 ± 0.3 (with an outlier value of −4.2 for ING-tmut). These values indicate a low confidence compared to those commonly found for smaller ligands (score < −1.5) [72], such as lipids or drug-like molecules [24,80]. However, they are in the same range of the confidence scores (in between −3.5 and −4.0) that we recently reported for peptides mimicking the NLSs of three PADI isoforms (i.e., PADI1, PADI2, and PADI3) targeting Impα3 [73]. Similar results were also obtained when PADI4 was the target protein, with peptides derived from the ubiquitin ligase MDM2 and including both wild-type and citrullinated species [21]. No appreciable difference or trend could be detected in our simulations for the confidence scores obtained in the docking of the different ING peptide species (either wild-type or with a single, double, and triple citrullination, and with the sole exception of the ING-tmut binding to PADI4). These findings support the observation of the common ability of the ING peptides binding to both Impα3 and PADI4 even in the presence of multiple PTMs, although we were not able to detect any measurable heat in the binding reactions of most of the peptides to PADI4 (Section 'ING peptides were capable of binding to PADI4').

The use of simulation methods was not further pursued to refine the docking poses obtained, to estimate the free energy in the association process, or to identify the individual contributions of specific amino acid residues to the binding (either in the two proteins or in the ING peptides). There were several distinct reasons for this. First, the diffusion-based algorithm of DiffDock leads to a stochastic search with a degree of variability, and with intrinsic uncertainties that are difficult to evaluate. Second, in our experiments *in vitro*, the ING peptides showed a disordered nature that suggests a large degree of conformational freedom even in their bound structure. Third, the final conformation of the ING peptides bound to the proteins evidenced small local steric clashes or distortions that required a post-docking energy minimization, leading to further uncertainties on the fine details of the anchoring poses. It should also be noted that the output of DiffDock does not provide the location of hydrogen atoms, which were added in the energy minimization procedure. More importantly, while DiffDock does not have a limit on the number of degrees of freedom of the ligand being docked, both its training and typical use are restricted to relatively small molecules, and its accuracy is degraded for our 23-residue disordered peptides.

In summary, the large number of degrees of freedom of the ING peptides hampered an exhaustive sampling of their bound conformations, but the indications of the simulations point out distinctly to the binding of all the peptides to the hot-spot regions of both Impα3 and PADI4. It is worth to stress that these results were obtained in a large search volume due to the size of both proteins, and in a completely blind docking protocol. We care to interpret the docking poses obtained not as the actual 'best' anchoring configuration (i.e., as the one it might be obtained if crystallography or cryo-electron microscopy could be used), but as an indication of the propensity for the ING peptides to target the expected protein binding sites. In fact, the peptide conformations obtained could more reasonably represent intermediates in the first steps of the protein/peptide association process. In the case of Impα3, we already noted that this points out to an induced-fit binding mechanism that favors the recognition of NLS regions [81], which could indicate that binding to importins is not a two-state process (probably explaining some of the differences among the apparent K_d values obtained by BLI and those obtained by the other techniques). A similar mechanism may also apply to PADI4. Nevertheless, the induced-fit mechanism hypothesized for the binding to both proteins should be confirmed through experimental validation, due to limitations in the sampling accuracy of the docking algorithm mentioned above.

The association rate constants, k_{on}, approximately correlated with charge mixing in the peptide sequence

Since the peptides were disordered (as it is the NLS region in the intact ING4 [29]), we tested whether the use of some recent resources for the analysis of disordered protein sequences could give further insights into the properties of the citrullinated peptides. To that end we used CIDER [76], which based on the sequence alone predicts the NCPR (i.e., net charge per residue), FCR (i.e, the fraction of charged residues) and the parameter κ, that describes the sequence patterning of oppositely charged residues. The value of κ ranges in between 0 and 1: low values of κ correspond to primary sequence where positively and negatively charges are well-mixed through the sequence. For the ING peptides, the predicted κ values were: 0.199 (ING-wt), 0.202 (ING-mut1), 0.162 (ING-mut2), 0.153 (ING-mut3), 0.155 (ING-dmut1), 0.145 (ING-dmut2), 0.140 (ING-dmut3) and 0.121 (ING-tmut).

For the ING peptides, a linear relationship was found between the number of citrullines and FCR and NCPR, which is obviously due to the fact that a positive charge is lost any time an Arg is being modified (in our case to a Gln, which has equivalent properties to citrulline in this context). However, we also found a non-trivial linear

relationship between the values of k_{on} (for any of the three proteins) and κ, which is approximate and best evident for Impα3 (Figure S10).

This finding may be reporting that the well-mixing of positive and negative charges in the sequence of the NLSs helps to achieve a good speed of binding to any protein. We are fully aware that these linear relationships could be only hold for this particular sequence, and then, further analysis of disordered NLSs and their binding to other proteins are necessary to show the full utility of these relationships. On the other hand, several members of the class of monopartite NLSs (i.e., those binding only to the NLS major binding site) possess a combination of basic and acidic residues, and bipartite NLSs (i.e., those binding simultaneously to both the NLS major and minor binding site of importins) have optimal patterns with an alternation of acidic and basic/hydrophobic residues in the central and terminal region, respectively [82]. Therefore, at least for Impα3, our findings could be due to the particular features of the binding hot-spot of this protein. However, it is also known that the conformations of intrinsically disordered polypeptides in solution are influenced by the linear sequence distributions of oppositely charged residues [83], with marked differences between polyampholytes and polyelectrolytes. In turn, such conformational propensities could lead to increasing differences in the binding process. Then, the association rate constants might also directly depend upon the pattern of charges in the peptide sequences, besides the specific protein they are targeting.

Discussion

ING4 is a member of the inhibitor of growth (ING) family that has a role in cell cycle control, cell proliferation, cell differentiation, cell migration, stem cell maintenance, apoptosis, DNA damage response, replication, angiogenesis, hypoxia, apoptosis and autophagy [84,85]. ING4 expression is ubiquitous in human tissues, but ING4 down-regulation is often observed in various types of cancers [85]. ING4 protein has a short half-life in the cells and it is degraded through the ubiquitin–proteasome pathway [25,84–86]. It is mainly located in the nucleus, where it is transported by importins with the help of a bipartite NLS in its primary structure. This region is required not only for nuclear translocation, but it is also the hot-spot for the cancer-promoting protein from Epstein-Barr virus, EBNA3C [87], and it is also involved in binding to p53 [34] Furthermore, PADI4 also binds to this region and citrullinates arginine residues at that polypeptide patch resulting in inhibition of: (i) p53 binding; (ii) its acetylation; and (iii) p21 expression [42]. Interestingly enough, the binding of PADI4 stabilizes ING4, but its citrullination promotes its degradation [86]. In this work, we tried to determine how citrullination affected the binding of the NLS region to Impα3 and PADI4.

Our results suggest that as the degree of citrullination increased, the binding to either Impα3 species or PADI4 decreased, and thus citrullination interfered with the binding. In the case of PADI4 the results were more dramatic, as the presence of a citrulline, at any position in the ING peptide, did not allow to measure any heat exchanged during the binding (Table 2 and Section 'ING peptides were capable of binding to PADI4'). A similar conclusion i.e., the binding affinity decreased as the citrullination increased was obtained with PADI4 and different citrullinated species of peptides derived from MDM2 [21], although in MDM2 complete binding disruption is only observed for the double citrullinated peptide, and it is not detected for the single modified ones. Then, it seems that although the general trend is that citrullination decreased the binding to PADI4, differences in the sequences of the substrate regions could modulate the binding when PTMs were occurring. From the point of view of PADI4, it seems comprehensible that citrullination interferes with binding, since a positive (Arg) residue is removed, and the enzymatic product should have less affinity for the enzyme. In the case of ING peptides, a single citrullination, at any of the three possible Arg positions, seemed to be enough to lead to the impossibility of measuring a heat exchanged with the environment during the binding reaction (Section 'ING peptides were capable of binding to PADI4'), although binding appeared to occur, as measured by BLI (Table 4) and by our *in silico* experiments (Figures 7 and 8). At this stage, it is important to further pinpoint that the K_d values from BLI (Tables 3 and 4) are upper estimations of the real dissociation constants, since they were obtained assuming a two-state process (free and bound polypeptides) for the binding of each peptide to the proteins. If we assume that there are more than those two species as it seems to be suggested by the docking results (Section 'ING peptides targeted the NLS binding site of importin species and the active site of PADI4') and the presence of an induced-fit mechanism for the peptide binding to the importin species then the equilibrium dissociation constant cannot be obtained as $K_d = k_{off}/k_{on}$, but rather by using more complex relationships [79]. From the point of view of Impα3, the variation in the affinity with the degree of citrullination could be rationalized as due to the loss of a positive charge, which favorably binds within its cargo binding site, because NLSs frequently contain sequences rich in positively charged amino acids such as Arg residues [88]. At the best of our knowledge, our results are the first describing the effects *in vitro* of citrullination in the binding to importins. We have tried to compare the k_{on} and k_{off} values (Table 4) with those of other peptides, either citrullinated or wild-type, derived from MDM2 which also bind to PADI4

[21]. In the case of MDM2, the k_{on} rates values ranged from 0.018 to 0.06 μM^{-1} s^{-1}, but there was not a clear relationship between the degree of citrullination and the value of the association rate as that observed in Table 4 for ING peptides. On the other hand, the k_{off} rates were in the range 0.039–0.28 s^{-1}, instead of being nearly constant as those observed in this work. Then, it seems that it is not possible to obtain a simple relationship among the association and dissociation kinetic rates of citrullinated peptides coming from different protein sequences. We have also tried to compare the k_{on} and k_{off} values of the binding to both importin species of the differently modified ING peptides with those previously reported in the literature [18,73]. As it happens with the binding to PADI4, it was not possible to obtain a simple relationship among the different sequences from peptides from several proteins.

It is important to emphasize that our conclusions have been obtained from *in vitro* results and therefore, any biological implication must be considered as a hypothesis. Our approach is robust since it allows to study how successive citrullination can interfere with binding to importin α3 (as a representative member of the importin family) and its deletion mutant without the IBB, and at the best of our knowledge it is not possible to control in any cell-based experiment how many arginines can be citrullinated by PADI4 (or other isoform). For instance, a cell-based citrullination study of HIF-1 α by PADI4 yielded six arginine sites which could be modified, but it was not specified whether such citrullination was sequential or simultaneous [89]. Furthermore, cell-based citrullination studies of ING4 by PADI4 have shown simultaneous citrullination signals at the two N-terminal domains of ING4 (and therefore, at least two arginines are citrullinated) [42]. In addition, PADI1, another isoform of the PADI family, in cell-based experiments citrullinated AKT2 simultaneously at three different arginines [90]. In our approach *in vitro*, we can control the number of residues modified and then, we can get reliable conclusions on: (i) how many citrullines are necessary to interfere with the binding to PADI4, or alternatively to Imp α3; and, (ii) how the presence of citrullines can modulate the binding to those proteins from distinct kinetic and thermodynamic points of view.

It is important to pinpoint that we have used Impα3 as a paradigm carrier for nuclear translocation, due to the reasons indicated above (Section 'Introduction'); however, at the best of our knowledge there is no evidence that such protein is the sole transporter of ING4 to drive its nuclear translocation. It could be that under extensive citrullination, other nuclear transporter proteins could get involved in translocating ING4.

Since the NLS of ING4 is the region also used to interact with p53, and cell-based experiments have shown that citrullination, in spite of the unknown number of modified arginines, hampers p53-binding [34,86], it is tempting to hypothesize that if Impα3 is the sole protein in charge of nuclear-translocating ING4, then, within the cell, citrullination of its NLS region might interfere with such translocation. However, we do not know whether such measured reduction *in vitro* (a 4-fold reduction from ING-wt to ING-tmut, Table 2) in a cell environment would be sufficient to interfere with such binding, and furthermore, we do not know for sure the biological significance of such difference in the cell, because of: (i) the crowding effect within the cell, which could alter the affinity value measured *in vitro* (Table 2); (ii) experiments with peptides provide a simplified perspective, but conformational propensities and steric hindrance in the full length may further contribute by amplifying small effects; and (iii) if even other importin isoforms could be at a high cellular concentrations, many of them would not be available for ING4, as most of them would be loaded with other cargo proteins, given the large number of molecules to be internalized in the nucleus. Thus, if most of the importins were occupied in translocating other cargos, a small difficulty such as a minor reduction in affinity, as that reported in Table 2, would be relevant to reduce the efficiency of the binding. The biological effect of a given reduction in affinity in a certain interaction will depend on the actual concentrations of the proteins involved, and the maximal effect of this reduced affinity will occur at concentrations around or lower than the dissociation constant. Regulation of physiological processes do not necessarily involve an all-or-none modulation, but a delicate and intricate balance between concomitant processes, and, as indicated, the binding of ING4 to importin α3 is taking place within a cellular context in which many other potential cargo proteins would compete for binding. In any case, the biological effect of sequential citrullination on ING4 will be pursued in future work.

Finally, it is important to indicate that our findings suggest that citrullination can be a way to modulate the loss of function of ING4. Thus, citrullination, as a cellular insult, adds to acetylation [91–94]; SUMOylation [95–98]; and phosphorylation [39,99–101] in the portfolio of PTMs capable of modulating nuclear translocation. The important difference is that citrullination involves Arg as the amino acid subjected to modification (instead of Lys, Thr or Ser in the other PTMs mentioned above) through an irreversible process, whereas for the rest of the described PTMs a hydrolysis can revert the modification. The mechanistic differences caused by the citrullination, when compared with acetylation and phosphorylation, are important because citrullination is an irreversible process, which cannot be reverted by a simple hydrolysis (to date there are not known de-citrullinating enzymes, but deacetylases and phosphorylases are well-known). Furthermore, the citrullination

removes a positive charge, as acetylation does, but it does not introduce a bulky side-chain (as the methyl group of the acetyl moiety). And phosphorylation introduces at least one negative charge (at physiological pH), in contrast to the disappearance of a positive one. Thus, citrullination changes completely the electrostatic and hydrophobic properties of the surroundings of the modified residue, potentially altering conformational and functional propensities. We also demonstrated that the isolated ING peptides, which contain the NLS of ING4, were disordered and did not have any propensity to acquire α-helix- or turn-like conformations (Figures 1 and 2). The NLS region within full-length ING is also disordered [29], and it seems that this intrinsic disorder is a key determinant of the ability of the NLS region to interact with several targets. Previous studies with other NLSs of intrinsically disordered proteins [39–41] or of well-folded proteins [18,37,38], have suggested an inhibitory action of the IBB in Impα3: this domain hampers the anchoring of the NLS of the corresponding cargo protein into the major NLS-binding region of Impα3. In this context, from the ITC results, we have not observed a much stronger binding affinity of the eight NLSs regions for ΔImpα3 compared to Impα3 (Table 2), in disagreement with the findings obtained for other NLS peptides assayed before [39–41].

It could be thought that since there are several examples in the literature of tyrosine residues involved in the protein–protein interface of some complexes [102–104], the additional tyrosine we put in all the peptides at the C-terminus, to allow for a reliable determination of their concentrations, could modulate their binding to both importin species. However, in our simulations, we did not find any evidence that may suggest that the C-terminal tyrosine forms a close contact with any of the residues of importin, or form any hydrogen-bonded atom with the phenolic group of its aromatic ring. Even for other NLS peptides whose crystallographic complex with importin has been solved (i.e., RanBP3 and LSD1, reported in PDB entries 5XZX and 7JJM, respectively [69,105]), only the core anchoring motif has the atomic coordinates solved. This suggests that the terminal parts of these NLS peptides remains 'fuzzy' when they are bound, in spite of the fact that both contain tyrosine residues (residue Tyr47 in PDB entry 5ZZX has the side chain not solved, and the whole Tyr120 in PDB entry 7JJM is reported as "MISSING RESIDUE" [69,105]). Then, we believe that the presence of the C-terminal tyrosine in the ING peptides is not altering the measured affinity constants as determined by ITC or BLI.

The fact that ING-wt binds to the active site of PADI4 as shown by the *in silico* results (Figures 7 and 8) and the colorimetric assays (Figure S9), suggests that this peptide might be used to block the citrullination of the intact ING4. Citrullination of ING4 promotes its degradation, leading to the impossibility of modulating the activity of p53, among other functions [86]. By assuming that the affinity of intact ING4 for PADI4 is similar to that of ING-wt, we could use the latter as a bait to block the citrullination of ING4, and the peptide could be considered a lead compound to develop a new anticancer drug, with a K_d in the low micromolar range that might be used as a starting point. We do not suggest that the peptide, in its current polypeptide sequence, could surpass other well-known inhibitors of PADI4 activity, as GSK484 used in our work (Figure S9), but rather, that with extensive modifications it might be used as a lead compound to inhibit PADI4 activity. However, it is important to indicate that this proposed use has a key caveat, as ING-wt (and also the citrullinated peptides) was capable of binding to Impα3 with a similar affinity (Tables 2, 3 and 4, and Section 'ING peptides were capable of binding to PADI4'). Therefore, binding of other proteins to be translocated towards the nucleus would be affected as well, which is an off-target effect that would need to be reduced during its pharmacological optimization process.

To sum up, we have shown that the degree of citrullination in the disordered NLS region of ING could interfere with its nuclear translocation. Such degree of citrullination also interfered with the binding to PADI4.

CRediT authorship contribution statement

María Gabriela Álvarez-Rodríguez: Writing – review & editing, Investigation, Formal analysis. **Sonia Vega:** Investigation, Formal analysis. **Felipe Hornos:** Writing – review & editing, Investigation, Formal analysis. **Augusto Fienco-Bacusoy:** Investigation, Formal analysis. **Olga Abian:** Formal analysis. **Adrian Velazquez-Campoy:** Writing – review & editing, Writing – original draft, Supervision, Project administration, Methodology, Investigation, Funding acquisition, Formal analysis, Conceptualization. **Bruno Rizzuti:** Writing – review & editing, Writing – original draft, Supervision, Project administration, Methodology, Investigation, Funding acquisition, Formal analysis, Conceptualization. **José L. Neira:** Writing – review & editing, Writing – original draft, Supervision, Project administration, Methodology, Investigation, Funding acquisition, Formal analysis, Conceptualization.

DATA AVAILABILITY

Data will be made available on request.

DECLARATION OF COMPETING INTEREST

The authors declare that they have no known competing financial interests or personal

relationships that could have appeared to influence the work reported in this paper.

Acknowledgements

This research was funded by Ministerio de Ciencia, Innovación y Universidades MCIN/AEI/10.13039/501100011033/ and "ERDF A way of Making Europe" [PID2021-127296OB-I00 and PID2024-160408OB-I00 to AVC]; Consellería de Educación, Cultura, Universidades y Empleo (Generalitat Valenciana) [CIACO/2024/17 to JLN and AVC]. This research was also funded by Next Generation EU program, Italian PNNR, Mission 4, Component 2, Investment 1.5, "Innovation Ecosystems" project Tech4You, "Technologies for Climate Change Adaptation and Quality of Life Improvement" [CUP B83C22003980006 to BR]; and by HORIZON European Union [EXPLORA GA n° 101181841 to JLN and FH]. MGAR was supported by EXPLORA GA n° 101181841.
The funders had no role in the study design, data collection and analysis, decision to publish, or preparation of the manuscript.
We thank the two anonymous reviewers for helpful suggestions, discussions and corrections. We thank Dr. Shixian Lin for handling the manuscript.

Appendix A. Supplementary material

Ten figures showing: the methyl region of the 1D-^{1}H NMR spectra of some of the ING peptides (Figure S1); the amide regions of the 1D-^{1}H NMR spectra of some of the ING peptides (Figures S2 and S3); the ITC results for ΔImpα3 and the eight ING peptides (Figure S4); the sensorgrams of the ING-wt peptide to each of the importin species at selected concentrations (Figure S5); the fluorescence titration curves of some selected ING peptides with PADI4 (Figure S6); the pseudo-first order plots for the binding of PADI4 to some selected ING peptides (Figure S7); the sensorgrams of the ING-wt and ING-mut1 peptides to PADI4 (Figure S8); the results of the COLDER assays with and without antipyrine in the presence of ING-wt (Figure S9); and the approximate linear relationships of the kinetic parameters of binding with the disorder parameter κ of the sequence (Figure S10). Eight tables containing the ^{1}H NMR assignments of the ING peptides (Tables ST1–ST8). Supplementary material to this article can be found online at https://doi.org/10.1016/j.jmb.2026.169877.

Received 9 March 2026;
Accepted 18 May 2026;
Available online 21 May 2026

Keywords:
PADI proteins;
importin proteins;
nuclear localization signal;
calorimetry;
fluorescence

† These two authors contributed equally to this work.

Abbreviations:
ARM, armadillo; BAEE, N-α-Benzoyl-L-arginine ethyl ester; BLI, biolayer interferometry; COLDER, color developed reagent; DIPSI, decoupling in the presence of scalar interactions; DOSY, diffusion ordered spectroscopy; FCR, fraction of charged residues; IBB, importin β-binding domain; Impα3, human importin α3 isoform (residues 1–521); ΔImpα3, IBB-depleted species of Impα3 (residues 64–521 of the intact protein); ING4, inhibitor of growth 4; ING-wt, peptide comprising the nuclear localization signal of the intact wild-type ING4, encompassing residues Lys130-Glu152; ING-mut1, modified peptide comprising residues Lys130-Glu152 of ING4, with a citrulline at Arg132; ING-mut2, modified peptide comprising residues Lys130-Glu152 of ING4, with a citrulline at Arg142; ING-mut3, modified peptide comprising residues Lys130-Glu152 of ING4, with a citrulline at Arg144; ING-dmut1, double modified peptide comprising residues Lys130-Glu152 of ING4, with two citrullines at Arg132 and Arg142; ING-dmut2, double modified peptide comprising residues Lys130-Glu152 of ING4, with two citrullines at Arg132 and Arg144; ING-dmut3, double modified peptide comprising residues Lys130-Glu152 of ING4, with two citrullines at Arg142 and Arg144; ING-tmut, triple modified peptide comprising residues Lys130-Glu152 of ING4, with three citrullines at Arg132, Arg142 and Arg144; ITC, isothermal titration calorimetry; MW, molecular weight; NCPR, net charge *per* residue; NLS, nuclear localization signal; NMR, nuclear magnetic resonance; NOESY, nuclear Overhauser effect spectroscopy; NPC, nuclear pore complex; PADI, peptidyl arginine iminohydrolase; PTM, post-translational modification; TCEP, tris(2-carboxyethyl)phosphine; TOCSY, total correlation spectroscopy; TSC, thiosemicarbazide; TSP, 3-(trimethylsilyl) propionic acid-2,2,3,3-$^{2}H_4$-sodium salt; UV, ultraviolet

References

[1]. Senshu, T., Akiyama, K., Ishigami, A., Nomura, K., (1999). Studies on specificity of peptidylarginine deiminase reactions using an immunochemical probe that recognizes an enzymatically deiminated partial sequence of mouse keratin K1. *J. Dermatol. Sci.* **21**, 113–126. https://doi.org/10.1016/S0923-1811(99)00026-2.

[2]. Asaga, H., Yamada, M., Senshu, T., (1998). Selective deimination of vimentin in calcium ionophore-induced apoptosis of mouse peritoneal macrophages. *Biochem. Biophys. Res. Commun.* **243**, 641–646. https://doi.org/10.1006/bbrc.1998.8148.

[3]. Cuthbert, G.L., Daujat, S., Snowden, A.W., Erdjument-Bromage, H., Hagiwara, T., Yamada, M., Schneider, R., Gregory, P.D., Tempst, P., Bannister, A.J., Kouzarides, T., (2004). Histone deimination antagonizes arginine methylation. *Cell* **118**, 545–553. https://doi.org/10.1016/j.cell.2004.08.020.

[4]. Ishigami, A., Maruyama, N., (2010). Importance of research on peptidylarginine deiminase and citrullinated proteins in age-related disease. *Geriatr. Gerontol. Int.* **10**, S53–S58. https://doi.org/10.1111/J.1447-0594.2010.00593.X.

[5]. Wang, Y., Wysocka, J., Sayegh, J., Lee, Y.H., Pertin, J. R., Leonelli, L., Sonbuchner, L.S., McDonald, C.H., Cook, R.G., Dou, Y., Roeder, R.G., Clarke, S., Stallcup, M.R., Allis, C.D., Coonrod, S.A., (1979). Human PAD4 regulates histone arginine methylation levels via demethylimination. *Science* **306** (2004), 279–283. https://doi.org/10.1126/SCIENCE.1101400.

[6]. Wang, Y., Chen, R., Gan, Y., Ying, S., (2021). The roles of PAD2- and PAD4-mediated protein citrullination catalysis in cancers. *Int. J. Cancer* **148**, 267–276. https://doi.org/10.1002/IJC.33205.

[7]. György, B., Tóth, E., Tarcsa, E., Falus, A., Buzás, E.I., (2006). Citrullination: a posttranslational modification in health and disease. *Int. J. Biochem. Cell Biol.* **38**, 1662–1677. https://doi.org/10.1016/J.BIOCEL.2006.03.008.

[8]. Anzilotti, C., Pratesi, F., Tommasi, C., Migliorini, P., (2010). Peptidylarginine deiminase 4 and citrullination in health and disease. *Autoimmun. Rev.* **9**, 158–160. https://doi.org/10.1016/j.autrev.2009.06.002.

[9]. Zhu, C., Liu, C., Chai, Z., (2023). Role of the PADI family in inflammatory autoimmune diseases and cancers: a systematic review. *Front. Immunol.* **14** https://doi.org/10.3389/FIMMU.2023.1115794.

[10]. Kizawa, K., Takahara, H., Troxler, H., Kleinert, P., Mochida, U., Heizmann, C.W., (2008). Specific citrullination causes assembly of a globular S100A3 homotetramer: a putative Ca^{2+} modulator matures human hair cuticle. *J. Biol. Chem.* **283**, 5004–5013. https://doi.org/10.1074/JBC.M709357200.

[11]. Neira, J.L., Araujo-Abad, S., Cámara-Artigas, A., Rizzuti, B., Abian, O., Giudici, A.M., Velazquez-Campoy, A., de Juan Romero, C., (2022). Biochemical and biophysical characterization of PADI4 supports its involvement in cancer. *Arch. Biochem. Biophys.* **717**, 109125. https://doi.org/10.1016/J.ABB.2022.109125.

[12]. Slade, D.J., Horibata, S., Coonrod, S.A., Thompson, P. R., (2014). A novel role for protein arginine deiminase 4 in pluripotency: the emerging role of citrullinated histone H1 in cellular programming. *Bioessays* **36**, 736–740. https://doi.org/10.1002/BIES.201400057;SUBPAGE:STRING:FULL.

[13]. Witalison, E., Thompson, P., Hofseth, L., (2015). Protein arginine deiminases and associated citrullination: physiological functions and diseases associated with dysregulation. *Curr. Drug Targets* **16**, 700–710. https://doi.org/10.2174/1389450116666150202160954.

[14]. Yang, C., Dong, Z.Z., Zhang, J., Teng, D., Luo, X., Li, D., Zhou, Y., (2021). Peptidylarginine deiminases 4 as a promising target in drug discovery. *Eur. J. Med. Chem.* **226** https://doi.org/10.1016/j.ejmech.2021.113840.

[15]. Ying, S., Dong, S., Kawada, A., Kojima, T., Chavanas, S., Méchin, M.C., Adoue, V., Serre, G., Simon, M., Takahara, H., (2009). Transcriptional regulation of peptidylarginine deiminase expression in human keratinocytes. *J. Dermatol. Sci.* **53**, 2–9. https://doi.org/10.1016/J.JDERMSCI.2008.09.009.

[16]. Li, P., Wang, D., Yao, H., Doret, P., Hao, G., Shen, Q., Qiu, H., Zhang, X., Wang, Y., Chen, G., Wang, Y., (2010). Coordination of PAD4 and HDAC2 in the regulation of p53-target gene expression. *Oncogene* **29**, 3153–3162. https://doi.org/10.1038/ONC.2010.51;SUBJMETA=100,1244,200,208,2285,45,612,631;KWRD=GENE+REGULATION, HISTONE+POST-TRANSLATIONAL+MODIFICATIONS, TUMOUR-SUPPRESSOR+PROTEINS.

[17]. Li, P., Yao, H., Zhang, Z., Li, M., Luo, Y., Thompson, P. R., Gilmour, D.S., Wang, Y., (2008). Regulation of p53 target gene expression by peptidylarginine deiminase 4. *Mol. Cell Biol.* **28**, 4745–4758. https://doi.org/10.1128/MCB.01747-07;SUBPAGE:STRING:ACCESS.

[18]. Neira, J.L., Rizzuti, B., Abián, O., Araujo-Abad, S., Velázquez-Campoy, A., de Juan Romero, C., (2022). Human enzyme PADI4 binds to the nuclear carrier importin α3. *Cells* **11** https://doi.org/10.3390/CELLS11142166.

[19]. Araujo-Abad, S., Rizzuti, B., Vidal, M., Abian, O., Fárez-Vidal, M.E., Velazquez-Campoy, A., de Juan Romero, C., Neira, J.L., (2024). Unveiling the binding between the armadillo-repeat domain of plakophilin 1 and the intrinsically disordered transcriptional repressor RYBP. *Biomolecules* **14** https://doi.org/10.3390/BIOM14050561.

[20]. Araujo-Abad, S., Rizzuti, B., Villamarin-Ortiz, A., Pantoja-Uceda, D., Moreno-Gonzalez, C.M., Abian, O., Velazquez-Campoy, A., Neira, J.L., de Juan Romero, C., (2023). New insights into cancer: MDM2 binds to the citrullinating enzyme PADI4. *Protein Sci.* **32**, e4723. https://doi.org/10.1002/PRO.4723;CTYPE:STRING:JOURNAL.

[21]. Neira, J.L., Rizzuti, B., Palomino-Schätzlein, M., Rejas, V., Abian, O., Velazquez-Campoy, A., (2025). Citrullination at the N-terminal region of MDM2 by the PADI4 enzyme. *Protein Sci.* **34** https://doi.org/10.1002/PRO.70033.

[22]. Araujo-Abad, S., Fuentes-Baile, M., Rizzuti, B., Bazán, J.F., Villamarin-Ortiz, A., Saceda, M., Fernández, E., Vidal, M., Abian, O., Velazquez-Campoy, A., de Juan Romero, C., Neira, J.L., (2023). The intrinsically disordered, epigenetic factor RYBP binds to the citrullinating enzyme PADI4 in cancer cells. *Int. J. Biol. Macromol.* **246**, 125632. https://doi.org/10.1016/J.IJBIOMAC.2023.125632.

[23]. Araujo-Abad, S., Rizzuti, B., Soto-Conde, L., Vidal, M., Abian, O., Velazquez-Campoy, A., Neira, J.L., de Juan Romero, C., (2024). Citrullinating enzyme PADI4 and transcriptional repressor RING1B bind in cancer cells. *Int. J. Biol. Macromol.* **274** https://doi.org/10.1016/J.IJBIOMAC.2024.133163.

[24]. Araujo-Abad, S., García-Peñarrubia, B., Giudici, A.M., Neira, J.L., Rizzuti, B., de Juan Romero, C., Poveda, J. A., (2025). The citrullinating enzyme PADI4 binds to lipids: identification of new target interactions for cancer therapy. *J. Mol. Biol.* **437** https://doi.org/10.1016/j.jmb.2025.169297.

[25]. Russell, M., Berardi, P., Gong, W., Riabowol, K., (2006). Grow-ING, Age-ING and Die-ING: ING proteins link

cancer, senescence and apoptosis. *Exp. Cell Res.* **312**, 951–961. https://doi.org/10.1016/j.yexcr.2006.01.020.

[26]. Kim, S., Chin, K., Gray, J.W., Bishop, J.M., (2004). A screen for genes that suppress loss of contact inhibition: identification of ING4 as a candidate tumor suppressor gene in human cancer. *PNAS* **101**, 16251–16256. https://doi.org/10.1073/pnas.0407158101.

[27]. Moreno, A., Palacios, A., Orgaz, J.L., Jimenez, B., Blanco, F.J., Palmero, I., (2010). Functional impact of cancer-associated mutations in the tumor suppressor protein ING4. *Carcinogenesis* **31**, 1932–1938. https://doi.org/10.1093/carcin/bgq171.

[28]. Du, Y., Cheng, Y., Su, G., (2019). The essential role of tumor suppressor gene ING4 in various human cancers and non-neoplastic disorders. *Biosci. Rep.* **39** https://doi.org/10.1042/BSR20180773.

[29]. Culurgioni, S., Mũoz, I.G., Palacios, A., Redondo, P., Blanco, F.J., Montoya, G., (2010). Crystallization and preliminary X-ray diffraction analysis of the dimerization domain of the tumour suppressor ING4. *Acta Crystallogr. Sect. F Struct. Biol. Cryst. Commun.* **66**, 567–570. https://doi.org/10.1107/S1744309110010080.

[30]. Palacios, A., Garcia, P., Padró, D., López-Hernández, E., Martín, I., Blanco, F.J., (2006). Solution structure and NMR characterization of the binding to methylated histone tails of the plant homeodomain finger of the tumour suppressor ING4. *FEBS Letters* **580**, 6903–6908. https://doi.org/10.1016/j.febslet.2006.11.055.

[31]. Culurgioni, S., Muñoz, I.G., Moreno, A., Palacios, A., Villate, M., Palmero, I., Montoya, G., Blanco, F.J., (2012). Crystal structure of inhibitor of growth 4 (ING4) dimerization domain reveals functional organization of ING family of chromatin-binding proteins. *J. Biol. Chem.* **287**, 10876–10884. https://doi.org/10.1074/jbc.M111.330001.

[32]. Palacios, A., Moreno, A., Oliveira, B.L., Rivera, T., Prieto, J., García, P., Fernández-Fernández, M.R., Bernadó, P., Palmero, I., Blanco, F.J., (2010). The dimeric structure and the bivalent recognition of H3K4me3 by the tumor suppressor ING4 suggests a mechanism for enhanced targeting of the HBO1 complex to chromatin. *J. Mol. Biol.* **396**, 1117–1127. https://doi.org/10.1016/j.jmb.2009.12.049.

[33]. Palacios, A., Muñoz, I.G., Pantoja-Uceda, D., Marcaida, M.J., Torres, D., Martín-García, J.M., Luque, I., Montoya, G., Blanco, F.J., (2008). Molecular basis of histone H3K4me3 recognition by ING4. *J. Biol. Chem.* **283**, 15956–15964. https://doi.org/10.1074/jbc.M710020200.

[34]. Zhang, X., Wang, K.S., Wang, Z.Q., Xu, L.S., Wang, Q.W., Chen, F., Wei, D.Z., Han, Z.G., (2005). Nuclear localization signal of ING4 plays a key role in its binding to p53. *Biochem. Biophys. Res. Commun.* **331**, 1032–1038. https://doi.org/10.1016/j.bbrc.2005.04.023.

[35]. Stewart, M., (2007). Molecular mechanism of the nuclear protein import cycle. *Nature Rev. Mol. Cell Biol.* **8**, 195–208. https://doi.org/10.1038/NRM2114.

[36]. Bednenko, J., Cingolani, G., Gerace, L., (2003). Nucleocytoplasmic transport: navigating the channel. *Traffic* **4**, 127–135. https://doi.org/10.1034/J.1600-0854.2003.00109.X.

[37]. Kobe, B., (1999). Autoinhibition by an internal nuclear localization signal revealed by the crystal structure of mammalian importin α. *Nature Struct. Biol.* **6**, 388–397. https://doi.org/10.1038/7625.

[38]. Smith, K.M., Tsimbalyuk, S., Edwards, M.R., Cross, E. M., Batra, J., Soares da Costa, T.P., Aragão, D., Basler, C.F., Forwood, J.K., (2018). Structural basis for importin alpha 3 specificity of W proteins in Hendra and Nipah viruses. *Nature Commun.* **9** https://doi.org/10.1038/S41467-018-05928-5.

[39]. Neira, J.L., Rizzuti, B., Jiménez-Alesanco, A., Palomino-Schätzlein, M., Abián, O., Velázquez-Campoy, A., Iovanna, J.L., (2020). A phosphorylation-induced switch in the nuclear localization sequence of the intrinsically disordered NUPR1 hampers binding to importin. *Biomolecules* **10**, 1–22. https://doi.org/10.3390/BIOM10091313.

[40]. Neira, J.L., Rizzuti, B., Jiménez-Alesanco, A., Abián, O., Velázquez-Campoy, A., Iovanna, J.L., (2020). The paralogue of the intrinsically disordered nuclear protein 1 has a nuclear localization sequence that binds to human importin α3. *Int. J. Mol. Sci.* **21** https://doi.org/10.3390/ijms21197428.

[41]. Neira, J.L., Jiménez-Alesanco, A., Rizzuti, B., Velazquez-Campoy, A., (2021). The nuclear localization sequence of the epigenetic factor RYBP binds to human importin α3. *Biochim. Biophys. Acta Proteins Proteom.* **1869** https://doi.org/10.1016/J.BBAPAP.2021.140670.

[42]. Guo, Q., Fast, W., (2011). Citrullination of Inhibitor of Growth 4 (ING4) by Peptidylarginine Deminase 4 (PAD4) disrupts the interaction between ING4 and p53. *J. Biol. Chem.* **286**, 17069–17078. https://doi.org/10.1074/jbc.M111.230961.

[43]. Díaz-García, C., Hornos, F., Giudici, A.M., Cámara-Artigas, A., Luque-Ortega, J.R., Arbe, A., Rizzuti, B., Alfonso, C., Forwood, J.K., Iovanna, J.L., Gómez, J., Prieto, M., Coutinho, A., Neira, J.L., (2020). Human importin α3 and its N-terminal truncated form, without the importin-β-binding domain, are oligomeric species with a low conformational stability in solution. *Biochim. Biophys. Acta Gen. Subj.* **1864** https://doi.org/10.1016/j.bbagen.2020.129609.

[44]. Gill, S.C., von Hippel, P.H., (1989). Calculation of protein extinction coefficients from amino acid sequence data. *Anal. Biochem.* **182**, 319–326. https://doi.org/10.1016/0003-2697(89)90602-7.

[45]. Neira, J.L., Hornos, F., Bacarizo, J., Cámara-Artigás, A., Gómez, J., (2016). The monomeric species of the regulatory domain of tyrosine hydroxylase has a low conformational stability. *Biochemistry* **55**, 3418–3431. https://doi.org/10.1021/ACS.BIOCHEM.6B00135/SUPPL_FILE/BI6B00135_SI_001.PDF.

[46]. Birdsall, B., King, R.W., Wheeler, M.R., Lewis, C.A., Goode, S.R., Dunlap, R.B., Roberts, G.C.K., (1983). Correction for light absorption in fluorescence studies of protein-ligand interactions. *Anal. Biochem.* **132**, 353–361. https://doi.org/10.1016/0003-2697(83)90020-9.

[47]. Royer, C.A., Scarlata, S.F., (2008). Chapter 5 fluorescence approaches to quantifying biomolecular interactions. *Methods Enzymol.* **450**, 79–106. https://doi.org/10.1016/S0076-6879(08)03405-8.

[48]. Beckett, D., (2011). Measurement and analysis of equilibrium binding titrations: a beginner's guide. *Methods Enzymol.* **488**, 1–16. https://doi.org/10.1016/B978-0-12-381268-1.00001-X.

[49]. J. Cavanagh, W.J. Fairbrother, A.G. Palmer, N.J. Skelton, Protein NMR Spectroscopy: Principles and Practice (second ed.), 2007.
[50]. Piotto, M., Saudek, V., Sklenář, V., (1992). Gradient-tailored excitation for single-quantum NMR spectroscopy of aqueous solutions. *J. Biomol. NMR* **2**, 661–665. https://doi.org/10.1007/BF02192855.
[51]. Wilkins, D.K., Grimshaw, S.B., Receveur, V., Dobson, C. M., Jones, J.A., Smith, L.J., (1999). Hydrodynamic radii of native and denatured proteins measured by pulse field gradient NMR techniques. *Biochemistry* **38**, 16424–16431. https://doi.org/10.1021/BI991765Q.
[52]. Marion, D., Wüthrich, K., (1983). Application of phase sensitive two-dimensional correlated spectroscopy (COSY) for measurements of ^{1}H-^{1}H spin-spin coupling constants in proteins. *Biochem. Biophys. Res. Commun.* **113**, 967–974. https://doi.org/10.1016/0006-291X(83)91093-8.
[53]. Bax, A., Davis, D.G., (1969). MLEV-17-based two-dimensional homonuclear magnetization transfer spectroscopy. *J. Magn. Reson.* **65** (1985), 355–360. https://doi.org/10.1016/0022-2364(85)90018-6.
[54]. Kumar, A., Ernst, R.R., Wüthrich, K., (1980). A two-dimensional nuclear Overhauser enhancement (2D NOE) experiment for the elucidation of complete proton-proton cross-relaxation networks in biological macromolecules. *Biochem. Biophys. Res. Commun.* **95**, 1–6. https://doi.org/10.1016/0006-291X(80)90695-6.
[55]. Cavanagh, J., Rance, M., (1969). Suppression of cross-relaxation effects in TOCSY spectra via a modified DIPSI-2 mixing sequence. *J. Magn. Reson.* **96** (1992), 670–678. https://doi.org/10.1016/0022-2364(92)90357-D.
[56]. Wüthrich, K., (1986). NMR of Proteins and Nucleic Acids. Academic Press, New York.
[57]. Kjaergaard, M., Poulsen, F.M., (2011). Sequence correction of random coil chemical shifts: correlation between neighbor correction factors and changes in the Ramachandran distribution. *J. Biomol. NMR* **50**, 157–165. https://doi.org/10.1007/S10858-011-9508-2/METRICS.
[58]. Kjaergaard, M., Brander, S., Poulsen, F.M., (2011). Random coil chemical shift for intrinsically disordered proteins: effects of temperature and pH. *J. Biomol. NMR* **49**, 139–149. https://doi.org/10.1007/S10858-011-9472-X/METRICS.
[59]. Vega, S., Abian, O., Velazquez-Campoy, A., (2015). A unified framework based on the binding polynomial for characterizing biological systems by isothermal titration calorimetry. *Methods* **76**, 99–115. https://doi.org/10.1016/j.ymeth.2014.09.010.
[60]. Knipp, M., Vašák, M., (2000). A colorimetric 96-well microtiter plate assay for the determination of enzymatically formed citrulline. *Anal. Biochem.* **286**, 257–264. https://doi.org/10.1006/abio.2000.4805.
[61]. Kearney, P.L., Bhatia, M., Jones, N.G., Yuan, L., Glascock, M.C., Catchings, K.L., Yamada, M., Thompson, P.R., (2005). Kinetic characterization of protein arginine deiminase 4: a transcriptional corepressor implicated in the onset and progression of rheumatoid arthritis. *Biochemistry* **44**, 10570–10582. https://doi.org/10.1021/BI050292M.
[62]. Sugawara, K., Yoshizawa, Y., Tzeng, S., Epstein, W.L., Fukuyama, K., (1998). Colorimetric determination of citrulline residues in proteins. *Anal. Biochem.* **265**, 92–96. https://doi.org/10.1006/ABIO.1998.2925.
[63]. Holm, A., Rise, F., Sessler, N., Sollid, L.M., Undheim, K., Fleckenstein, B., (2006). Specific modification of peptide-bound citrulline residues. *Anal. Biochem.* **352**, 68–76. https://doi.org/10.1016/j.ab.2006.02.007.
[64]. Frenzel, D., Willbold, D., (2014). Kinetic titration series with biolayer interferometry. *PLoS One* **9**, e106882. https://doi.org/10.1371/JOURNAL.PONE.0106882.
[65]. Edwards, P.R., Maule, C.H., Leatherbarrow, R.J., Winzor, D.J., (1998). Second-order kinetic analysis of IAsys biosensor data: its use and applicability. *Anal. Biochem.* **263**, 1–12. https://doi.org/10.1006/abio.1998.2814.
[66]. Hall, D.R., Gorgani, N.N., Altin, J.G., Winzor, D.J., (1997). Theoretical and experimental considerations of the pseudo-first-order approximation in conventional kinetic analysis of IAsys biosensor data. *Anal. Biochem.* **253**, 145–155. https://doi.org/10.1006/abio.1997.2358.
[67]. O'Shannessy, D.J., Winzor, D.J., (1996). Interpretation of deviations from pseudo-first-order kinetic behavior in the characterization of ligand binding by biosensor technology. *Anal. Biochem.* **236**, 275–283. https://doi.org/10.1006/abio.1996.0167.
[68]. Pantoja-Uceda, D., Neira, J.L., Saelices, L., Robles-Rengel, R., Florencio, F.J., Muro-Pastor, M.I., Santoro, J., (2016). Dissecting the binding between glutamine synthetase and its two natively unfolded protein inhibitors. *Biochemistry* **55**, 3370–3382. https://doi.org/10.1021/ACS.BIOCHEM.6B00072.
[69]. Koyama, M., Matsuura, Y., (2017). Crystal structure of importin-α3 bound to the nuclear localization signal of Ran-binding protein 3. *Biochem. Biophys. Res. Commun.* **491**, 609–613. https://doi.org/10.1016/j.bbrc.2017.07.155.
[70]. Horikoshi, N., Tachiwana, H., Saito, K., Osakabe, A., Sato, M., Yamada, M., Akashi, S., Nishimura, Y., Kagawa, W., Kurumizaka, H., (2011). Structural and biochemical analyses of the human PAD4 variant encoded by a functional haplotype gene. *Acta Crystallogr. D Biol. Crystallogr.* **67**, 112–118. https://doi.org/10.1107/S0907444910051711.
[71]. Pettersen, E.F., Goddard, T.D., Huang, C.C., Couch, G. S., Greenblatt, D.M., Meng, E.C., Ferrin, T.E., (2004). UCSF Chimera–a visualization system for exploratory research and analysis. *J. Comput. Chem.* **25**, 1605–1612. https://doi.org/10.1002/JCC.20084.
[72]. Corso, G., Stärk, H., Jing, B., Barzilay, R., Jaakkola, T., (2022). DiffDock: diffusion steps, twists, and turns for molecular docking. *arXiv* (accessed September 8, 2024) https://arxiv.org/abs/2210.01776v2.
[73]. Neira, J.L., Abian, O., Velazquez-Campoy, A., Rizzuti, B., (2026). Unveiling nuclear localization signals in human arginine deiminase proteins. *Protein Sci.* **35** https://doi.org/10.1002/PRO.70517.
[74]. Wang, J., Wolf, R.M., Caldwell, J.W., Kollman, P.A., Case, D.A., (2004). Development and testing of a general Amber force field. *J. Comput. Chem.* **25**, 1157–1174. https://doi.org/10.1002/jcc.20035.
[75]. Humphrey, W., Dalke, A., Schulten, K., (1996). VMD: visual molecular dynamics. *J. Mol. Graph.* **14**, 33–38. https://doi.org/10.1016/0263-7855(96)00018-5.

[76]. Holehouse, A.S., Das, R.K., Ahad, J.N., Richardson, M. O.G., Pappu, R.V., (2017). CIDER: resources to analyze sequence-ensemble relationships of intrinsically disordered proteins. *Biophys. J.* **112**, 16–21. https://doi.org/10.1016/j.bpj.2016.11.3200.

[77]. Pace, C.N., Schmid, F.X., (1997). How to determine the molar absorbance coefficient of a protein. *Protein Struct.*, 253–260. https://doi.org/10.1093/OSO/9780199636198.003.0010.

[78]. Danielsson, J., Jarvet, J., Damberg, P., Gräslund, A., (2002). Translational diffusion measured by PFG-NMR on full length and fragments of the Alzheimer Aβ(1–40) peptide. Determination of hydrodynamic radii of random coil peptides of varying length. *Magn. Reson. Chem.* **40**, S89–S97. https://doi.org/10.1002/MRC.1132.

[79]. A. Fersht, Structure and mechanism in protein science: a guide to enzyme catalysis and protein folding, (2017) 631.

[80]. Álvarez-Rodríguez, M.G., Estaras, M., Hornos, F., Rizzuti, B., Santofimia-Castaño, P., Iovanna, J.L., Neira, J.L., (2026). Evaluating the therapeutic role of salvianolic acid a on pancreatic cancer cells through interaction with the intrinsically disordered protein NUPR1. *Int. J. Biol. Macromol.* **337** https://doi.org/10.1016/j.ijbiomac.2025.149435.

[81]. Hornos, F., Rizzuti, B., Neira, J.L., (2025). Importin α3 is tolerant to nuclear localization signal chirality. *Int. J. Mol. Sci.* **26** https://doi.org/10.3390/IJMS26167818.

[82]. Kosugi, S., Hasebe, M., Matsumura, N., Takashima, H., Miyamoto-Sato, E., Tomita, M., Yanagawa, H., (2009). Six classes of nuclear localization signals specific to different binding grooves of importinα. *J. Biol. Chem.* **284**, 478–485. https://doi.org/10.1074/jbc.M807017200.

[83]. Das, R.K., Pappu, R.V., (2013). Conformations of intrinsically disordered proteins are influenced by linear sequence distributions of oppositely charged residues. *PNAS* **110**, 13392–13397. https://doi.org/10.1073/pnas.1304749110.

[84]. Zhang, R., Jin, J., Shi, J., Hou, Y., (2017). INGs are potential drug targets for cancer. *J. Cancer Res. Clin. Oncol.* **143**, 189–197. https://doi.org/10.1007/s00432-016-2219-z.

[85]. Shatnawi, A., Abu Rabe, D.I., Frigo, D.E., (2021). Roles of the tumor suppressor inhibitor of growth family member 4 (ING4) in cancer. *Adv. Cancer Res.* **152**, 225–262. https://doi.org/10.1016/bs.acr.2021.05.004.

[86]. Tsai, K.W., Tseng, H.C., Lin, W.C., (2008). Two wobble-splicing events affect ING4 protein subnuclear localization and degradation. *Exp. Cell Res.* **314**, 3130–3141. https://doi.org/10.1016/j.yexcr.2008.08.002.

[87]. Saha, A., Bamidele, A., Murakami, M., Robertson, E.S., (2011). EBNA3C attenuates the function of p53 through interaction with inhibitor of growth family proteins 4 and 5. *J. Virol.* **85**, 2079–2088. https://doi.org/10.1128/jvi.02279-10.

[88]. Lu, J., Wu, T., Zhang, B., Liu, S., Song, W., Qiao, J., Ruan, H., (2021). Types of nuclear localization signals and mechanisms of protein import into the nucleus. *Cell Commun. Signal* **19** https://doi.org/10.1186/s12964-021-00741-y.

[89]. Chen, R., Lin, Z., Shen, S., Zhu, C., Yan, K., Suo, C., Liu, R., Wei, H., Gao, L., Fan, K., Zhang, H., Sun, L., Gao, P., (2024). Citrullination modulation stabilizes HIF-1α to promote tumour progression. *Nature Commun.* **15** https://doi.org/10.1038/S41467-024-51882-W.

[90]. Xue, T., Liu, X., Song, C., Fei, S., Gu, J., Han, Y., Xing, J., Liu, X., Liang, F., Thompson, P.R., Zhang, X., (2025). Citrullination of AKT2 catalyzed by PAD1 facilitates the maintenance of stemness characteristics of ovarian cancer stem-like cells in ovarian cancer. *Adv. Sci. (Weinh)* **12** https://doi.org/10.1002/ADVS.202501014.

[91]. Ko, Y.H., Lokareddy, R.K., Doll, S.G., Yeggoni, D.P., Girdhar, A., Mawn, I., Klim, J.R., Rizvi, N.F., Meyers, R., Gillilan, R.E., Guo, L., Cingolani, G., (2024). Single acetylation-mimetic mutation in TDP-43 nuclear localization signal disrupts importin α1/β signaling. *J. Mol. Biol.* **436** https://doi.org/10.1016/j.jmb.2024.168751.

[92]. di Bari, M.G., Ciuffini, L., Mingardi, M., Testi, R., Soddu, S., Barilà, D., (2006). c-Abl acetylation by histone acetyltransferases regulates its nuclear-cytoplasmic localization. *EMBO Rep.* **7**, 727–733. https://doi.org/10.1038/SJ.EMBOR.7400700.

[93]. Fujimoto, H., Ikuta, T., Koike, A., Koike, M., (2023). Acetylation of the nuclear localization signal in Ku70 diminishes the interaction with importin-α. *Biochem. Biophys. Rep.* **33** https://doi.org/10.1016/j.bbrep.2022.101418.

[94]. Madison, D.L., Yaciuk, P., Kwok, R.P.S., Lundblad, J.R., (2002). Acetylation of the adenovirus-transforming protein E1A determines nuclear localization by disrupting association with importin-α. *J. Biol. Chem.* **277**, 38755–38763. https://doi.org/10.1074/jbc.M207512200.

[95]. Johansson, B.B., Fjeld, K., Solheim, M.H., Shirakawa, J., Zhang, E., Keindl, M., Hu, J., Lindqvist, A., Døskeland, A., Mellgren, G., Flatmark, T., Njølstad, P.R., Kulkarni, R.N., Wierup, N., Aukrust, I., Bjørkhaug, L., (2017). Nuclear import of glucokinase in pancreatic beta-cells is mediated by a nuclear localization signal and modulated by SUMOylation. *Mol. Cell. Endocrinol.* **454**, 146–157. https://doi.org/10.1016/j.mce.2017.06.020.

[96]. MacNeil, D.E., Lambert-Lanteigne, P., Qin, J., McManus, F.P., Bonneil, E., Thibault, P., Autexier, C., (2021). SUMOylation- and GAR1-dependent regulation of dyskerin nuclear and subnuclear localization. *Mol. Cell Biol.* **41** https://doi.org/10.1128/MCB.00464-20.

[97]. Lin, Q., Yu, B., Wang, X., Zhu, S., Zhao, G., Jia, M., Huang, F., Xu, N., Ren, H., Jiang, Q., Zhang, C., (2020). K6-linked SUMOylation of BAF regulates nuclear integrity and DNA replication in mammalian cells. *PNAS* **117**, 10378–10387. https://doi.org/10.1073/PNAS.1912984117.

[98]. Riley, B.E., Zoghbi, H.Y., Orr, H.T., (2005). SUMOylation of the polyglutamine repeat protein, ataxin-1, is dependent on a functional nuclear localization signal. *J. Biol. Chem.* **280**, 21942–21948. https://doi.org/10.1074/jbc.M501677200.

[99]. Wing, C.E., Chook, Y.M., (2026). Multiple roads between the nucleus and the cytoplasm: classes of linear NLSs and NESs and their receptors. *Curr. Opin. Struct. Biol.* **98** https://doi.org/10.1016/j.sbi.2026.103244.

[100]. Zimmermann, M.T., Williams, M.M., Klee, E.W., Lomberk, G.A., Urrutia, R., (2019). Modeling post-translational modifications and cancer-associated mutations that impact the heterochromatin protein 1α-

importin α heterodimers. *Proteins* **87**, 904–916. https://doi.org/10.1002/PROT.25752.

[101]. Chu, I.M., Hengst, L., Slingerland, J.M., (2008). The Cdk inhibitor p27 in human cancer: prognostic potential and relevance to anticancer therapy. *Nature Rev. Cancer* **8**, 253–267. https://doi.org/10.1038/nrc2347.

[102]. Koide, S., Sidhu, S.S., (2009). The importance of being tyrosine: lessons in molecular recognition from minimalist synthetic binding proteins. *ACS Chem. Biol.* **4**, 325–334. https://doi.org/10.1021/CB800314V.

[103]. Espinoza-Fonseca, L.M., (2012). Aromatic residues link binding and function of intrinsically disordered proteins. *Mol. Biosyst.* **8**, 237–246. https://doi.org/10.1039/C1MB05239J.

[104]. Moreira, I.S., Martins, J.M., Ramos, R.M., Fernandes, P. A., Ramos, M.J., (1834). Understanding the importance of the aromatic amino-acid residues as hot-spots. *Biochim. Biophys. Acta Proteins Proteom.* **2013**, 404–414. https://doi.org/10.1016/j.bbapap.2012.07.005.

[105]. Tu, W.J., McCuaig, R.D., Tan, A.H.Y., Hardy, K., Seddiki, N., Ali, S., Dahlstrom, J.E., Bean, E.G., Dunn, J., Forwood, J., Tsimbalyuk, S., Smith, K., Yip, D., Malik, L., Prasanna, T., Milburn, P., Rao, S., (2020). Targeting nuclear LSD1 to reprogram cancer cells and reinvigorate exhausted T cells via a novel LSD1-EOMES switch. *Front. Immunol.* **11**, 537128. https://doi.org/10.3389/FIMMU.2020.01228/TEXT.